Angular values of linear dynamical systems and their connection to the dichotomy spectrum

Wolf-Jürgen Beyn* Thorsten Hüls*

Abstract. This work continues the investigation of the previously defined angular values (cf. [6]) for linear nonautonomous dynamical systems in finite dimensions. The s-th angular value measures the maximal average rotation which the dynamics exerts on s-dimensional subspaces. Our main theorem relates the angular values to the well-known dichotomy (or Sacker-Sell) spectrum and its associated spectral bundles. In particular, a reduction theorem is proven which shows that instead of general subspaces it is sufficient to consider so-called trace spaces which have their basis in the spectral fibers. The reduction leads to an algorithm for computing angular values of dimensions one and two. The algorithm is applied to several examples of dimension up to 4, including a system of coupled oscillators.

Key words. Nonautonomous dynamical systems, angular value, ergodic average, Sacker-Sell spectrum, numerical approximation.

AMS subject classifications. 37C05, 37E45, 34D09, 65Q10.

1. Introduction.

In the previous paper [6], a concept of angular values was introduced for linear discrete time dynamical systems. The notion aims at measuring the average rotation of subspaces of arbitrary dimension caused by the dynamical system. Several notions for quantifying rotations in dynamical systems exist in the literature, notably the rotation number for circle homeomorphisms and more general maps and flows, see e.g. [2, 10, 23, 24]. However, there is a fundamental difference: while rotation numbers measure the oriented angle between vectors and image vectors in two-dimensional subspaces, angular values are based on the principal angles between subspaces (which always lie in $[0, \frac{\pi}{2}]$) rather than vectors, even in the one-dimensional case. In this way one loses information on orientation but gains applicability to general time discrete systems and to subspaces of arbitrary dimension. We refer to [6] for a further review of and comparison with the literature.

While [6] mainly deals with the autonomous case, this article provides deeper insight into angular values for nonautonomous systems and presents a general numerical algorithm. We consider a nonautonomous linear difference equation of the form

$$u_{n+1} = A_n u_n, \quad A_n \in \mathbb{R}^{d,d}, \quad n \in \mathbb{N}_0 \tag{1.1}$$

and assume throughout this paper that all matrices are invertible and A_n as well as A_n^{-1} are uniformly bounded. For the applications we think of (1.1) as the linearization of a nonlinear (non)autonomous dynamical system along a particular trajectory, see the coupled oscillator in Section 4.2.7.

*Department of Mathematics, Bielefeld University
beyn@math.uni-bielefeld.de, huels@math.uni-bielefeld.de

We define the solution operator Φ corresponding to (1.1) by

$$\Phi(n,m) = \begin{cases} A_{n-1} \cdot \ldots \cdot A_m, & \text{for } n > m, \\ I, & \text{for } n = m, \\ A_n^{-1} \cdot \ldots \cdot A_{m-1}^{-1}, & \text{for } n < m. \end{cases}$$

To keep this paper self-contained, some important definitions and estimates of angles from [6] are summarized in Section 2. Our different notions of an s-th angular value are based on the averages

$$\frac{1}{n} a_{k+1,k+n}(V), \quad a_{k+1,k+n}(V) = \sum_{j=k+1}^{k+n} \measuredangle(\Phi(j-1,0)V, \Phi(j,0)V), \quad k \geq 0, n \geq 1. \tag{1.2}$$

Here V is an element of the Grassmann manifold $\mathcal{G}(s,d)$ of s-dimensional subspaces of $\mathbb{R}^d$ and $\measuredangle(U,V)$ denotes the largest principal angle between two subspaces $U, V \in \mathcal{G}(s,d)$, see [15, Ch. 6.4.3]. There are several possibilities to pass to a limit in (1.2) and take the supremum over $V \in \mathcal{G}(s,d)$, for example

$$\bar{\theta}_s = \limsup_{n\to\infty} \frac{1}{n} \sup_{V\in\mathcal{G}(s,d)} a_{1,n}(V), \quad \hat{\theta}_s = \sup_{V\in\mathcal{G}(s,d)} \limsup_{n\to\infty} \frac{1}{n} a_{1,n}(V). \tag{1.3}$$

We call $\bar{\theta}_s$ the s-inner and $\hat{\theta}_s$ the s-outer angular value of the system. More precisely, the angular values will be given the attribute 'upper' due to the lim sup in (1.3), while 'lower' will then refer to taking the lim inf. Moreover, analogous uniform angular values are defined by first taking the supremum of $a_{k+1,k+n}(V)$ over $k \in \mathbb{N}_0$ and then proceeding as above, see Definition 2.6 for details. In general, all these notions turn out to be different for nonautonomous systems, cf. [6, Section 3.2].

Our numerical methods aim at computing outer angular values. In case system (1.1) is autonomous, i.e. $A_n = A$ for $n \in \mathbb{N}_0$, all eight angular values mentioned above agree for $s = 1$ under a weak assumption (see [6, Theorem 5.7]). Moreover, it is shown how to compute first angular values from orthogonal bases of invariant subspaces which belong to eigenvalues of A of the same modulus. This reduces the numerical effort substantially to a series of Schur decompositions and to one-dimensional optimization, see [6, Secton 6].

One major goal of this article is to develop a reduction theorem which generalizes the autonomous results to nonautonomous systems and to arbitrary subspace dimensions. We tackle this task in Section 3. It turns out that the dichotomy spectrum, also called the Sacker-Sell spectrum [27], and its accompanying spectral bundles take over the role of invariant subspaces from the autonomous case. With every element $V \in \mathcal{G}(s,d)$ we associate a subspace, called the trace space, which has the same dimension and which has a basis composed of vectors from the fibers. Our main reduction result Theorem 3.5 then states that the limit of $\frac{1}{n} a_{1,n}(V)$ from (1.2) for the given space V agrees with the corresponding limit for the trace space. Similar results are derived for the inner angular values ($s = 1$) and for uniform angular values ($s \geq 1$) in Sections 3.3 and 3.4.

The reduction theorem is the basis for the numerical algorithm which we propose in Section 4. Note that angular values are generally not attained in the most stable or most unstable directions of the trace spaces. Therefore, algorithms, which use forward iteration in one or the other way, tend to fail since they follow asymptotic dynamics. Instead, our algorithm consists of the following steps:

1. Compute an approximation of the dichotomy spectrum.
2. Compute the corresponding spectral bundles and obtain the trace spaces.
3. Determine the supremum of (1.2) w.r.t. the trace spaces and for large values of n.

The first two tasks are accomplished by using the techniques from [18]. We apply this algorithm to several models with a view to illustrate various aspects. A comparison between explicitly known angular values and the output of our algorithm is provided for cases $s = 1$ and $s = 2$. In addition, we present a geometric interpretation. For nonlinear models, such as a 3-dimensional extension of the Hénon system and a 4-dimensional system of coupled oscillators, we find that angular values coincide with the average angle between successive tangent spaces w.r.t. an invariant fiber. Furthermore, we discuss the stability problems raised by simple forward iteration of matrices and how we circumvent them. Finally, we observe that the first angular value may be greater equal or less than the second, depending on the example.

2. Basic definitions and properties.

To keep the article self-contained, we summarize in this section some important notions, definitions and results from [6].

2.1. Angles and subspaces.

Let us begin with a useful characterization of the angle between two subspaces V and W of $\mathbb{R}^d$, both having the same dimension k. Principal angles between these subspaces can be computed from the singular values of $V_B^\top W_B$, where the columns of V_B and $W_B \in \mathbb{R}^{d,k}$ form orthonormal bases of V and W, respectively, see [15, Ch.6.4.3]. The smallest singular value is the cosine of the largest principal angle which we denote by $\measuredangle(V, W)$. We further use the notion

$$\measuredangle(v, w) = \measuredangle(\operatorname{span}(v), \operatorname{span}(w)), \quad v, w \in \mathbb{R}^d, v, w \neq 0$$

in case the subspaces are one-dimensional.

The following proposition, cf. [6], gives an alternative characterization of $\measuredangle(V, W)$, which turns out to be essential for the analysis of angular values.

Proposition 2.1. *Let $V, W \subseteq \mathbb{R}^d$ be two k-dimensional subspaces. Then the following relation holds*

$$\measuredangle(V, W) = \max_{\substack{v \in V \\ v \neq 0}} \min_{\substack{w \in W \\ w \neq 0}} \measuredangle(v, w) = \arccos\Big(\min_{\substack{v \in V \\ \|v\|=1}} \max_{\substack{w \in W \\ \|w\|=1}} v^\top w \Big).$$

The next proposition summarizes some well-known properties of the Grassmannian

$$\mathcal{G}(k, d) = \{V \subseteq \mathbb{R}^d \text{ is a subspace of dimension } k\},$$

see [15, Ch.6.4.3], [21].

Proposition 2.2. *The Grassmannian $\mathcal{G}(k, d)$ is a compact smooth manifold of dimension $k(d - k)$ and a metric space with respect to*

$$d(V, W) = \|P_V - P_W\|,$$

where P_V, P_W are the orthogonal projections onto V and W, respectively. Moreover, the formula

$$d(V, W) = \sin(\measuredangle(V, W)), \quad V, W \in \mathcal{G}(k, d)$$

holds and $\measuredangle(V,W)$ *defines an equivalent metric on* $\mathcal{G}(k,d)$ *satisfying*

$$\frac{2}{\pi}\measuredangle(V,W) \le d(V,W) \le \measuredangle(V,W).$$

The following lemma from [6] is our main tool to estimate angles of vectors and subspaces in terms of norms.

Lemma 2.3.

i) For any two vectors $v, w \in \mathbb{R}^d$ *with* $\|v\| < \|w\|$ *the following holds*

$$\tan^2 \measuredangle(v+w, w) \le \frac{\|v\|^2}{\|w\|^2 - \|v\|^2}.$$

ii) Let $V \in \mathcal{G}(k,d)$ *and* $P \in \mathbb{R}^{d,d}$ *be such that for some* $0 \le q < 1$

$$\|(I-P)v\| \le q\|Pv\| \quad \forall v \in V.$$

Then $\dim(V) = \dim(PV)$ *and the following estimate holds*

$$\measuredangle(V, PV) \le \frac{q}{(1-q^2)^{1/2}}.$$

Finally, we state a linear algebra result which will provide the basic reduction step in Theorem 3.3. By $\mathcal{R}(P)$ and $\mathcal{N}(P)$ we denote the range and kernel of a matrix P, respectively.

Lemma 2.4. *Let* $V \in \mathcal{G}(k,d)$ *and let* P *be a projector in* $\mathbb{R}^d$*. Furthermore, let* Q *be any projector defined in* V *and with range* $V \cap \mathcal{R}(P)$*. Then the linear map*

$$L = I - P + Q : V \to (I-P)V \oplus (V \cap \mathcal{R}(P)) \tag{2.1}$$

is a bijection and there exists a constant $\rho > 0$ *such that*

$$\|P(I-Q)v\| \le \rho\|(I-P)(I-Q)v\| \quad \forall v \in V. \tag{2.2}$$

Proof. Note that the sum in (2.1) is direct since $(I-P)V \subseteq \mathcal{N}(P)$. For the same reason, if $Lv = 0$ for some $v \in V$, then $(I-P)v = 0$ and $Qv = 0$ holds. This shows $v \in V \cap \mathcal{R}(P) = \mathcal{R}(Q)$ and $v = Qv = 0$. Thus L is one to one. To show that L is onto, take any $u \in (I-P)V$ and $w \in V \cap \mathcal{R}(P)$. Then we have $u = (I-P)v$ for some $v \in V$, and defining $\tilde{v} = (I-Q)v + w \in V$, we obtain $L\tilde{v} = (I-P)(v+w-Qv) + Qw = (I-P)v + w = u + w$. To show the estimate (2.2) note that $0 = (I-P)(I-Q)v = (I-P)v$ for some $v \in V$ implies $v \in V \cap \mathcal{R}(P) = \mathcal{R}(Q)$ and thus $(I-Q)v = 0 = P(I-Q)v$. Then we obtain (2.2) from the elementary fact that two linear maps $A, B\colon V \to \mathbb{R}^d$ satisfy $\mathcal{N}(B) \subseteq \mathcal{N}(A)$ if and only if there exists a constant $C > 0$ such that $\|Av\| \le C\|Bv\|$ for all $v \in V$. ∎

Remark 2.5. *The last step of the proof is a special case of a result from functional analysis: Let* $A, B\colon X \to Y$ *be linear bounded operators between Banach spaces* X *and* Y*, then* A *is called relatively bounded by* B *if there exists a constant* $C > 0$ *such that* $\|Ax\| \le C\|Bx\|$ *for all* $x \in X$*; see [14, Ch.3.7]. The smallest constant of this type is*

$$\rho(A,B) = \inf\{C > 0 : \|Ax\| \le C\|Bx\| \quad \forall x \in X\} = \sup_{Bx \neq 0} \frac{\|Ax\|}{\|Bx\|}. \tag{2.3}$$

If B *is Fredholm one can show that* A *is relatively bounded by* B *iff* $\mathcal{N}(B) \subseteq \mathcal{N}(A)$.

2.2. Definition of angular values. Several different types of angular values have been proposed in [6]. This reference also contains illustrative examples and existence results, regarding the limits, defined below. Let us emphasize again that our notion of angular values avoids to specify any kind of orientation. We are dealing with discrete time systems and don't want to make any assumption on how a current subspace is moved to the next subspace in one time step. From our point of view, orientation based angles are more meaningful for continuous time dynamical systems.

Definition 2.6. *Let the nonautonomous system (1.1) be given. For $s \in \{1, \dots, d\}$ define the quantities*

$$a_{m,n}(V) = \sum_{j=m}^{n} \measuredangle(\Phi(j-1,0)V, \Phi(j,0)V) \quad m,n \in \mathbb{N},\ V \in \mathcal{G}(s,d). \tag{2.4}$$

i) The upper resp. lower s-th **inner angular value** *is defined by*

$$\bar{\theta}_s = \limsup_{n\to\infty} \frac{1}{n} \sup_{V\in\mathcal{G}(s,d)} a_{1,n}(V), \quad \underline{\theta}_s = \liminf_{n\to\infty} \frac{1}{n} \sup_{V\in\mathcal{G}(s,d)} a_{1,n}(V). \tag{2.5}$$

ii) The upper resp. lower s-th **outer angular value** *is defined by*

$$\hat{\theta}_s = \sup_{V\in\mathcal{G}(s,d)} \limsup_{n\to\infty} \frac{1}{n} a_{1,n}(V), \quad \hat{\underline{\theta}}_s = \sup_{V\in\mathcal{G}(s,d)} \liminf_{n\to\infty} \frac{1}{n} a_{1,n}(V).$$

iii) The upper resp. lower s-th **uniform inner angular value** *is defined by*

$$\begin{aligned} \bar{\theta}_{[s]} &= \lim_{n\to\infty} \frac{1}{n} \sup_{V\in\mathcal{G}(s,d)} \sup_{k\in\mathbb{N}_0} a_{k+1,k+n}(V), \\ \underline{\theta}_{[s]} &= \liminf_{n\to\infty} \frac{1}{n} \sup_{V\in\mathcal{G}(s,d)} \inf_{k\in\mathbb{N}_0} a_{k+1,k+n}(V). \end{aligned} \tag{2.6}$$

iv) The upper resp. lower s-th **uniform outer angular value** *is defined by*

$$\begin{aligned} \hat{\theta}_{[s]} &= \sup_{V\in\mathcal{G}(s,d)} \lim_{n\to\infty} \frac{1}{n} \sup_{k\in\mathbb{N}_0} a_{k+1,k+n}(V), \\ \hat{\underline{\theta}}_{[s]} &= \sup_{V\in\mathcal{G}(s,d)} \lim_{n\to\infty} \frac{1}{n} \inf_{k\in\mathbb{N}_0} a_{k+1,k+n}(V). \end{aligned}$$

We observe the following relations between these angular values for all $s = 1, \dots, d$.

$$\begin{array}{ccccccc} \hat{\underline{\theta}}_{[s]} & \leq & \hat{\underline{\theta}}_s & \leq & \hat{\theta}_s & \leq & \hat{\theta}_{[s]} \\ |\wedge & & |\wedge & & |\wedge & & |\wedge \\ \underline{\theta}_{[s]} & \leq & \underline{\theta}_s & \leq & \bar{\theta}_s & \leq & \bar{\theta}_{[s]} \end{array} \tag{2.7}$$

3. Relation to the dichotomy spectrum. We discuss in this section relations between angular values and the dichotomy spectrum. This particularly results in a computational approach for angular values. We start with a brief introduction, cf. [19], of the dichotomy spectrum which is also called the Sacker-Sell spectrum.

3.1. The dichotomy spectrum. The dichotomy spectrum, see [27] is based on the notion of an exponential dichotomy, cf. [17, 4, 22, 8, 9, 25]. In the following we recall its general definition for a discrete interval $\mathbb{I} \subset \mathbb{Z}$ which is unbounded above, and for a linear system (1.1) which is bounded invertible, i.e. there exists a $C > 0$ such that $\|A_n\|, \|A_n^{-1}\| \leq C$ for all $n \in \mathbb{I}$.

Definition 3.1. *The difference equation* (1.1) *has an* ***exponential dichotomy*** *(**ED** for short) on* $\mathbb{I}$*, if there exist constants* $K > 0, \alpha_s, \alpha_u \in (0,1)$ *and families of projectors* P_n^s*,* $P_n^u := I - P_n^s$*,* $n \in \mathbb{I}$ *such that*

(i) $P_n^{s,u}\Phi(n,m) = \Phi(n,m)P_m^{s,u}$ *for all* $n, m \in \mathbb{I}$.

(ii) For $n, m \in \mathbb{I}$*,* $n \geq m$ *the following estimates hold:*

$$\|\Phi(n,m)P_m^s\| \leq K\alpha_s^{n-m}, \quad \|\Phi(m,n)P_n^u\| \leq K\alpha_u^{n-m}.$$

The tuple $(K, \alpha_{s,u}, P_{\mathbb{I}}^{s,u} = (P_n^{s,u})_{n\in\mathbb{I}})$ *is called the dichotomy data.*

The dichotomy spectrum is constructed, using the scaled equation

$$u_{n+1} = \frac{1}{\gamma}A_n u_n, \quad n \in \mathbb{I}. \tag{3.1}$$

Spectrum and resolvent set are defined as follows:

$$\Sigma_{\mathrm{ED}} := \{\gamma > 0 : (3.1) \text{ has no ED on } \mathbb{I}\}, \qquad R_{\mathrm{ED}} := \mathbb{R}^{>0} \setminus \Sigma_{\mathrm{ED}}.$$

Assume that A_n is uniformly bounded w.r.t. $n \in \mathbb{I}$. The Spectral Theorem [5, Theorem 3.4] provides the decomposition $\Sigma_{\mathrm{ED}} = \bigcup_{i=1}^{\ell} \mathcal{I}_i$ of the dichotomy spectrum into $\ell \leq d$ intervals

$$\mathcal{I}_i = [\sigma_i^-, \sigma_i^+], \ i = 1, \ldots, \ell, \quad \text{where} \quad 0 < \sigma_\ell^- \leq \sigma_\ell^+ < \cdots < \sigma_1^- \leq \sigma_1^+.$$

The intervals $\mathcal{I}_i$, $i = 1, \ldots, \ell$ are called spectral intervals.
Correspondingly, the resolvent set is $R_{\mathrm{ED}} = \bigcup_{i=1}^{\ell+1} R_i$ with resolvent intervals

$$R_1 = (\sigma_1^+, \infty), \quad R_i = (\sigma_i^+, \sigma_{i-1}^-), \ i = 2, \ldots, \ell+1 \text{ with } \sigma_{\ell+1}^+ = 0$$

see Figure 3.1. In case $\sigma_i^- = \sigma_i^+$ for an $i \in \{1, \ldots, \ell\}$ the spectral interval $\mathcal{I}_i$ is an isolated point.

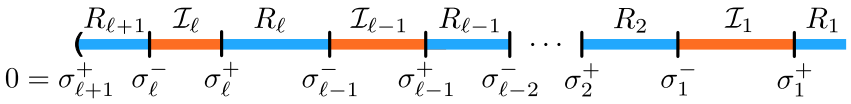

Figure 3.1: Illustration of spectral intervals (orange) and of resolvent intervals (blue).

For $\gamma \in R_i$ with $i \in \{1, \ldots, \ell+1\}$, the families of dichotomy projectors of (3.1) are denoted by $P_{\mathbb{I},i}^{s,u} = (P_{k,i}^{s,u})_{k\in\mathbb{I}}$. Note that these projectors are uniquely determined and that they have a hierarchical structure. For $n \in \mathbb{I}$ we obtain

$$\begin{aligned} \{0\} = \mathcal{R}(P_{n,\ell+1}^s) \subseteq \mathcal{R}(P_{n,\ell}^s) \subseteq \quad \cdots \subseteq \mathcal{R}(P_{n,1}^s) = \mathbb{R}^d, \\ \mathbb{R}^d = \mathcal{R}(P_{n,\ell+1}^u) \supseteq \mathcal{R}(P_{n,\ell}^u) \supseteq \quad \cdots \supseteq \mathcal{R}(P_{n,1}^u) = \{0\}. \end{aligned} \tag{3.2}$$

Spectral bundles that correspond to eigenspaces in autonomous systems are defined as follows (see Figure 3.2):

$$\mathcal{W}_n^i := \mathcal{R}(P_{n,i}^s) \cap \mathcal{R}(P_{n,i+1}^u), \quad i = 1, \dots, \ell. \tag{3.3}$$

Note that the dimensions of these spectral bundles $d_i := \dim(\mathcal{W}_n^i)$ for $i = 1, \dots, \ell$ do not depend on $n \in \mathbb{I}$. Alternatively, we may write the ranges of dichotomy projectors in terms of spectral bundles:

$$\mathcal{R}(P_{n,i}^u) = \bigoplus_{j=1}^{i-1} \mathcal{W}_n^j, \quad \mathcal{R}(P_{n,i}^s) = \bigoplus_{j=i}^{\ell} \mathcal{W}_n^j, \quad i = 1, \dots, \ell+1. \tag{3.4}$$

The fiber projector $\mathcal{P}_{n,i}, i = 1, \dots, \ell$ onto $\mathcal{W}_n^i$ along $\bigoplus_{\nu=1,\nu\neq i}^{\ell} \mathcal{W}_n^\nu$ is given by

$$\mathcal{P}_{n,i} = P_{n,i}^s P_{n,i+1}^u = P_{n,i+1}^u P_{n,i}^s = P_{n,i}^s - P_{n,i+1}^s = P_{n,i+1}^u - P_{n,i}^u. \tag{3.5}$$

Spectral bundles satisfy for $i = 1, \dots, \ell$ and $n, m \in \mathbb{I}$ the invariance condition

$$\Phi(n, m)\mathcal{W}_m^i = \mathcal{W}_n^i. \tag{3.6}$$

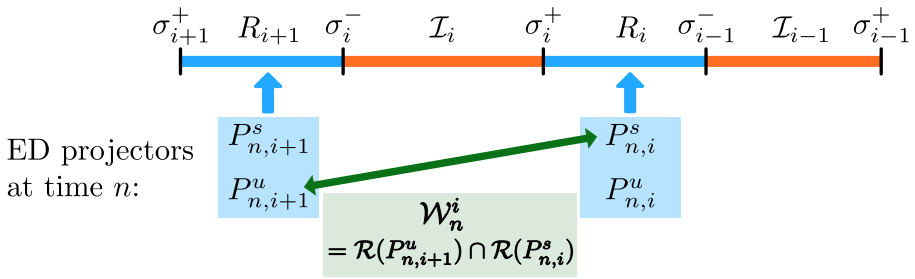

Figure 3.2: Construction of spectral bundles.

For $i \in \{2, \dots, \ell\}$ and $\gamma \in R_i = (\sigma_i^+, \sigma_{i-1}^-)$ the system (3.1) has an ED with

$$\begin{aligned} &\text{solution operator} \quad \Phi_\gamma(n, m) = \frac{1}{\gamma^{n-m}} \Phi(n, m), \\ &\text{projectors} \quad P_{n,i}^s, \qquad \text{constants} \quad \alpha_s(\gamma) = \frac{\sigma_i^+}{\gamma}, \quad \alpha_u(\gamma) = \frac{\gamma}{\sigma_{i-1}^-}. \end{aligned} \tag{3.7}$$

These satisfy for $n \geq m$ the ED-estimates

$$\begin{aligned} \|\Phi(n, m)P_{m,i}^s\| &\leq \gamma^{n-m} \|\Phi_\gamma(n, m)\| \leq K\gamma^{n-m} \left(\frac{\sigma_i^+}{\gamma}\right)^{n-m} = K(\sigma_i^+)^{(n-m)}, \\ \|\Phi(m, n)P_{n,i}^u\| &\leq \gamma^{m-n} \|\Phi_\gamma(m, n)\| \leq K\gamma^{m-n} \left(\frac{\gamma}{\sigma_{i-1}^-}\right)^{n-m} = K \left(\frac{1}{\sigma_{i-1}^-}\right)^{n-m}. \end{aligned}$$

Note that these estimates do not depend on the particular choice of $\gamma \in R_i$.

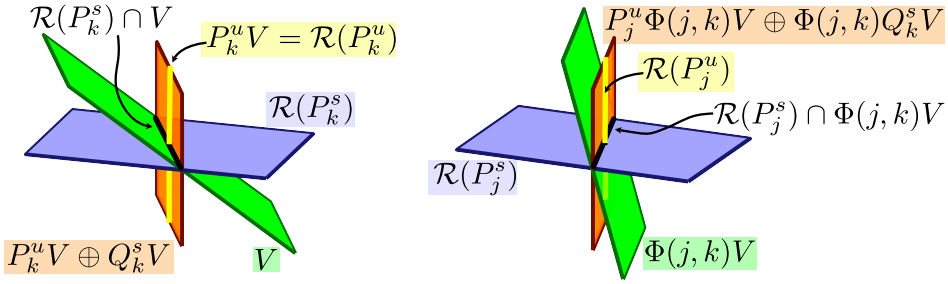

Figure 3.3: A subspace V (green) at time k (left) is driven by the dynamics at time $j > k$ (right) towards the direct sum (orange plane) of its unstable projection (yellow) and the intersection with the stable subspace (black).

3.2. Outer angular values and spectral bundles. In the remaining part of this section, we work in the setup $\mathbb{I} = \mathbb{N}_0$. As a first step, we prove that the dynamics of a dichotomic system drives a subspace (except for the intersection with its stable projection) towards its unstable projection, cf. Figure 3.3.

Theorem 3.2. *Let the system (1.1) have an exponential dichotomy on $\mathbb{N}_0$ with data $(K, \alpha_{s,u}, P_{\mathbb{N}_0}^{s,u})$. For $k \in \mathbb{N}_0$ and $V \in \mathcal{G}(s,d)$ let*

$$Q_k^s : V \to \mathcal{R}(P_k^s) \cap V \tag{3.8}$$

denote the orthogonal projector onto $\mathcal{R}(P_k^s) \cap V$. Then the quantity (recall (2.3))

$$\rho_k^s(V) = \inf\{C > 0 : \|P_k^s(I - Q_k^s)v\| \le C\|P_k^u(I - Q_k^s)v\| \ \forall v \in V\} < \infty$$

is finite and there exists an index $j_k^s = j_k^s(V)$ such that

$$K^2(\alpha_s\alpha_u)^{j_k^s}\rho_k^s(V) \le \frac{1}{2}. \tag{3.9}$$

For all $j \ge k + j_k^s$ the following estimate holds

$$\measuredangle(\Phi(j,k)V, \Phi(j,k)(P_k^u V \oplus Q_k^s V)) \le \frac{2}{\sqrt{3}}K^2(\alpha_s\alpha_u)^{j-k}\rho_k^s(V). \tag{3.10}$$

Proof. By Lemma 2.4 the quantity $\rho_k^s(V)$ is finite, and since $\alpha_s\alpha_u < 1$ there exists an index j_k^s satisfying (3.9). Our goal is to apply Lemma 2.3 (ii) for $j \ge k$ to the s-dimensional subspace $\tilde{V} = \Phi(j,k)V$ and the matrix $\tilde{P} = P_j^u + P_j^s\Phi(j,k)Q_k^s\Phi(k,j)$. First note that Lemma 2.4 and the properties of the solution operator imply

$$\begin{aligned}\Phi(j,k)(P_k^u V \oplus Q_k^s V) &= \Phi(j,k)(P_k^u + Q_k^s)\Phi(k,j)\Phi(j,k)V \\ &= (P_j^u + \Phi(j,k)Q_k^s\Phi(k,j))\Phi(j,k)V = \tilde{P}\tilde{V}.\end{aligned}$$

The exponential dichotomy yields for all $v \in V$ and $j \ge k$

$$\begin{aligned}\|P_k^u v\| &= \|\Phi(k,j)P_j^u\Phi(j,k)(P_k^u v + Q_k^s v)\| \\ &\le K\alpha_u^{j-k}\|\Phi(j,k)(P_k^u v + Q_k^s v)\| = K\alpha_u^{j-k}\|\tilde{P}\Phi(j,k)v\|, \\ \|(I - \tilde{P})\Phi(j,k)v\| &= \|\Phi(j,k)v - (\Phi(j,k)P_k^u v + \Phi(j,k)P_k^s Q_k^s v)\| \\ &= \|\Phi(j,k)P_k^s(I - Q_k^s)v\| \le K\alpha_s^{j-k}\|P_k^s(I - Q_k^s)v\|.\end{aligned}$$

Combining these estimates we obtain

$$\begin{aligned}\|(I-\tilde{P})\Phi(j,k)v\| &\le K\alpha_s^{j-k}\rho_k^s(V)\|P_k^u(I-Q_k^s)v\| = K\alpha_s^{j-k}\rho_k^s(V)\|P_k^u v\| \\ &\le K^2(\alpha_s\alpha_u)^{j-k}\rho_k^s(V)\|\tilde{P}\Phi(j,k)v\|.\end{aligned} \tag{3.11}$$

By condition (3.9) we can apply Lemma 2.3 (ii) with $q = K^2(\alpha_s\alpha_u)^{j-k}\rho_k^s(V) \le \frac{1}{2}$ for $j \ge k + j_k^s$,

$$\measuredangle(\Phi(j,k)V, \Phi(j,k)(P_k^u V \oplus Q_k^s V)) \le \frac{2K^2}{\sqrt{3}}(\alpha_s\alpha_u)^{j-k}\rho_k^s(V). \qquad \blacksquare$$

In a similar way, let

$$Q_k^u : V \to \mathcal{R}(P_k^u) \cap V \tag{3.12}$$

denote the orthogonal projector onto $\mathcal{R}(P_k^u) \cap V$. Then

$$\rho_k^u(V) = \inf\{C > 0 : \|P_k^u(I-Q_k^u)v\| \le C\|P_k^s(I-Q_k^u)v\| \ \forall v \in V\} < \infty$$

holds and there exists an index $j_k^u = j_k^u(V)$ such that

$$K^2(\alpha_s\alpha_u)^{j_k^u}\rho_k^u(V) \le \frac{1}{2}. \tag{3.13}$$

Then we obtain the following estimate for all $j \le k - j_k^u$,

$$\measuredangle(\Phi(j,k)V, \Phi(j,k)(P_k^s V \oplus Q_k^u V)) \le \frac{2}{\sqrt{3}}K^2(\alpha_s\alpha_u)^{k-j}\rho_k^u(V). \tag{3.14}$$

Theorem 3.2 provides the mechanism for reducing the analysis of angular values for general subspaces $V \in \mathcal{G}(s,d)$ to specific ones which have a basis consisting of vectors from the spectral bundle (3.3). For a fixed starting time $k \in \mathbb{N}$ and $i = 1, \dots, \ell$ we recall the projectors $\mathcal{P}_{k,i} = P_{k,i}^s P_{k,i+1}^u : \mathbb{R}^d \to \mathcal{W}_k^i$ from (3.5) and define the new projectors (cf. (3.2), (3.4), (3.8))

$$Q_{k,i}^s : V \to \mathcal{R}(P_{k,i}^s) \cap V, \quad i = 1, \dots, \ell. \tag{3.15}$$

For definiteness we assume the projector $Q_{k,i}^s$ to be orthogonal. With each $V \in \mathcal{G}(s,d)$ we associate its *trace space* having a fiber basis and defined by

$$\mathcal{T}_k(V) = \bigoplus_{i=1}^{\ell}(\mathcal{P}_{k,i}Q_{k,i}^s V) = \bigoplus_{i=1}^{\ell}(P_{k,i+1}^u(\mathcal{R}(P_{k,i}^s) \cap V)). \tag{3.16}$$

Below we will show $\dim \mathcal{T}_k(V) = s$ and the equality

$$\mathcal{T}_k(V) = \Big(\sum_{i=1}^{\ell}\mathcal{P}_{k,i}Q_{k,i}^s\Big)V. \tag{3.17}$$

The set of all such trace spaces is denoted by

$$\mathcal{D}_k(s,d) := \Big\{\bigoplus_{i=1}^{\ell} W_i : W_i \subseteq \mathcal{W}_k^i \text{ (subspace) } i = 1, \dots, \ell, \ \sum_{i=1}^{\ell}\dim W_i = s\Big\}. \tag{3.18}$$

Note that the equality $\mathcal{D}_k(s,d) = \{\mathcal{T}_k(V) : V \in \mathcal{G}(s,d)\}$ holds, since every $V = \bigoplus_{i=1}^{\ell} W_i \in \mathcal{D}_k(s,d)$ with $W_i \subseteq \mathcal{W}_k^i$ satisfies $\mathcal{P}_{k,i}Q_{k,i}^s V = W_i$, $i = 1, \dots, \ell$.

Our main reduction theorem is the following.

Theorem 3.3. *Assume that the difference equation (1.1) has the dichotomy spectrum* $\Sigma_{\mathrm{ED}} = \bigcup_{i=1}^{\ell}[\sigma_i^-, \sigma_i^+]$ *with fibers* $\mathcal{W}_k^i, i = 1\ldots,\ell$ *and projectors* $\mathcal{P}_{k,i}, i = 1,\ldots,\ell$, $k \in \mathbb{N}_0$. *Then for every* $k \in \mathbb{N}_0$ *and* $V \in \mathcal{G}(s,d)$, $s = 1,\ldots,d$ *there exists an index* $\overline{j} = \overline{j}(k,V)$ *and a constant* $C = C(k,V)$ *such that for all* $j \geq k + \overline{j}$ *the following estimate holds*

$$\measuredangle(\Phi(j,k)V, \Phi(j,k)\mathcal{T}_k(V)) \leq C(k,V)\Big(\max_{i=1,\ldots,\ell-1}\frac{\sigma_{i+1}^+}{\sigma_i^-}\Big)^{j-k}. \tag{3.19}$$

Remark 3.4. *Note that several of the spaces* $\mathcal{P}_{k,i}Q_{k,i}^s V$ *occurring in the decomposition (3.16) may be trivial. The following proof will show that one can then omit the corresponding quotients* $\frac{\sigma_{i+1}^+}{\sigma_i^-}$ *from the maximum in (3.19). Moreover, the proof will provide values for the index* $\overline{j}(k,V)$ *and the constant* $C(k,V)$.

Proof.
Step1: Let us first discuss a recursive construction that leads to the trace space (3.17). With every $V \in \mathcal{G}(s,d)$ we associate subspaces $V_i \in \mathcal{G}(s,d)$ and further projectors $\tilde{Q}_{k,i} (i = 1,\ldots,\ell+1)$ defined by $V_1 = V$, $\tilde{Q}_{k,1} = I_d$ and then for $i = 1,\ldots,\ell$ as follows

$$\begin{aligned} &\tilde{Q}_{k,i+1} : V_i \to \mathcal{R}(P_{k,i+1}^s) \cap V_i \quad \text{orthogonal projector,} \\ &V_{i+1} = P_{k,i+1}^u V_i \oplus \tilde{Q}_{k,i+1} V_i. \end{aligned} \tag{3.20}$$

Figure 3.4 illustrates this recursion for two characteristic cases.

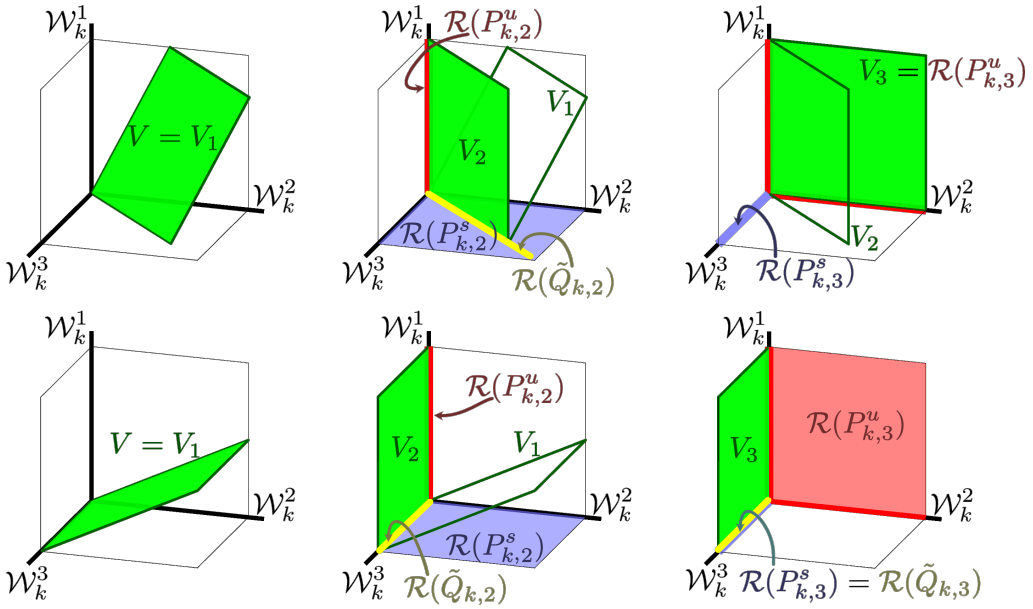

Figure 3.4: Recursive construction of subspaces, cf. (3.20) for two characteristic cases. Upper row: Since V intersects $\mathcal{W}_k^i$ only in $\{0\}$ for any $i \in \{1,2,3\}$, the sequence of subspaces $(V_i)_{i\leq 4}$ is constant for $i \geq 3$, i.e. $V_2 \neq V_3 = V_4$. Lower row: V has a nontrivial intersection with $\mathcal{W}_k^3$ and the sequence of subspaces $(V_i)_{i\leq 4}$ is constant for $i \geq 2$. In both cases, the trace space of V is given as $\mathcal{T}_k(V) = V_3$.

Note that Lemma 2.4 implies $V_{i+1} = (P^u_{k,i+1} + \tilde{Q}_{k,i+1})V_i$ and $\dim V_i = \dim V_{i+1}$. In addition, we claim for $i = 1, \dots, \ell$

$$P^u_{k,i+1}V_i = \big(\sum_{\nu=1}^{i} \mathcal{P}_{k,\nu}Q^s_{k,\nu}\big)V, \quad \tilde{Q}_{k,i+1}V_i = Q^s_{k,i+1}V. \tag{3.21}$$

We proceed by induction. First note that (3.2), (3.20) and (3.15) imply $P^s_{k,1} = I_d$, $Q_{k,1}V = \tilde{Q}_{k,1}V_1$. Further, we have by (3.5), (3.20), (3.15)

$$P^u_{k,2}V_1 = \mathcal{P}_{k,1}V, \quad \tilde{Q}_{k,2}V_1 = \mathcal{R}(P^s_{k,2}) \cap V = Q^s_{k,2}V.$$

Assume that (3.21) holds for the index i. Then we obtain from (3.20), (3.4)

$$\begin{aligned}
\tilde{Q}_{k,i+2}V_{i+1} &= \mathcal{R}(P^s_{k,i+2}) \cap V_{i+1} = \mathcal{R}(P^s_{k,i+2}) \cap (P^u_{k,i+1}V_i \oplus \tilde{Q}_{k,i+1}V_i) \\
&= \mathcal{R}(P^s_{k,i+2}) \cap \tilde{Q}_{k,i+1}V_i = \mathcal{R}(P^s_{k,i+2}) \cap (\mathcal{R}(P^s_{k,i+1}) \cap V) \\
&= \mathcal{R}(P^s_{k,i+2}) \cap V = Q^s_{k,i+2}V.
\end{aligned}$$

Furthermore,

$$\begin{aligned}
P^u_{k,i+2}V_{i+1} &= P^u_{k,i+2}(P^u_{k,i+1}V_i \oplus \tilde{Q}_{k,i+1}V_i) \\
&= P^u_{k,i+2}\Big(\big(\sum_{\nu=1}^{i} \mathcal{P}_{k,\nu}Q^s_{k,\nu}\big)V \oplus Q^s_{k,i+1}V\Big) \\
&= \big(\sum_{\nu=1}^{i} P^u_{k,i+2}\mathcal{P}_{k,\nu}Q^s_{k,\nu}\big)V + P^u_{k,i+2}P^s_{k,i+1}Q^s_{k,i+1}V.
\end{aligned}$$

From (3.2), (3.4) and (3.5) we have the equalities $P^u_{k,i+2}\mathcal{P}_{k,\nu} = \mathcal{P}_{k,\nu}$ for $\nu \le i$ and $P^u_{k,i+2}P^s_{k,i+1} = \mathcal{P}_{k,i+1}$. With $\mathcal{R}(\mathcal{P}_{k,i+1}) \cap \bigoplus_{\nu=1}^{i} \mathcal{W}^\nu_k = \{0\}$ this leads to

$$P^u_{k,i+2}V_{i+1} = \big(\sum_{\nu=1}^{i} \mathcal{P}_{k,\nu}Q^s_{k,\nu}\big)V \oplus \mathcal{P}_{k,i+1}Q^s_{k,i+1}V = \big(\sum_{\nu=1}^{i+1} \mathcal{P}_{k,\nu}Q^s_{k,\nu}\big)V.$$

The last equality needs an argument. The relation "$\supseteq$" is obvious. For the converse we consider $v, w \in V$ and construct $\tilde{v} \in V$ such that

$$\sum_{\nu=1}^{i} \mathcal{P}_{k,\nu}Q^s_{k,\nu}v + \mathcal{P}_{k,i+1}Q^s_{k,i+1}w = \sum_{\nu=1}^{i+1} \mathcal{P}_{k,\nu}Q^s_{k,\nu}\tilde{v}. \tag{3.22}$$

For this purpose set $\tilde{v} = v + Q^s_{k,i+1}(w - v)$ and verify (3.22) by using the equality $\mathcal{P}_{k,\nu}Q^s_{k,\nu}Q^s_{k,i+1}(w - v) = \mathcal{P}_{k,\nu}Q^s_{k,i+1}(w - v) = \mathcal{P}_{k,\nu}P^s_{k,i+1}Q^s_{k,i+1}(w - v) = 0$ for $\nu \le i$. In this way one also obtains the equality of the representations (3.16) and (3.17) via an induction w.r.t. the index i.

Step2: We prove the key estimate (3.19). Let us apply Theorem 3.2 for $i = 1, \dots, \ell$ to the scaled operator Φ_γ with $\gamma \in R_{i+1} = (\sigma^+_{i+1}, \sigma^-_i)$ and $V_i \in \mathcal{G}(s, d)$, $\tilde{Q}_{k,i}$ as defined by (3.20) (recall (3.7) and $\sigma^+_{\ell+1} = 0$). The index $j^s_{k,i}$ is determined by $2K^2\big(\frac{\sigma^+_{i+1}}{\sigma^-_i}\big)^{j^s_{k,i}}\rho^s_{k,i}(V) \le 1$ (cf. (3.9)) where, due to the second equation in (3.21),

$$\rho^s_{k,i}(V) = \inf\{C > 0 : \|P^s_{k,i+1}(I - Q^s_{k,i+1})v\| \le C\|P^u_{k,i+1}(I - Q^s_{k,i+1})v\| \ \forall v \in V\}.$$

Then the estimate (3.10) leads for $j \geq k + j^s_{k,i}$ and $i = 1 \dots, \ell$ to

$$\measuredangle(\Phi_\gamma(j,k)V_i, \Phi_\gamma(j,k)V_{i+1})) \leq \frac{2}{\sqrt{3}} K^2 \left(\frac{\sigma^+_{i+1}}{\sigma^-_i}\right)^{j-k} \rho^s_{k,i}(V).$$

Since angles do not depend on scalings we can replace Φ_γ by Φ in this estimate. Finally, observe $P^s_{k,\ell+1} = 0$, $Q^s_{k,\ell+1} = 0$ and thus $V_{\ell+1} = P^u_{k,\ell+1} V_\ell = V_\ell = \mathcal{T}_k(V)$ due to (3.21). The triangle inequality then yields for $j - k \geq \bar{j} = \max_{i=1,\dots,\ell} j^s_{k,i}$

$$\begin{aligned}\measuredangle(\Phi(j,k)V, \Phi(j,k)\mathcal{T}_k(V)) &\leq \sum_{i=1}^{\ell} \measuredangle(\Phi(j,k)V_i, \Phi(j,k)V_{i+1}) \\ &\leq \frac{2K^2}{\sqrt{3}} \left(\max_{i=1,\dots,\ell-1} \frac{\sigma^+_{i+1}}{\sigma^-_i}\right)^{j-k} \sum_{i=1}^{\ell} \rho^s_{k,i}(V). \qquad \blacksquare\end{aligned}$$

Some conclusions of Theorem 3.3 are summarized in Theorem 3.5 below. In particular, we present an important characterization of outer angular values $\underset{\wedge}{\theta}_1$, $\hat{\theta}_1$ if all spectral bundles are one-dimensional.

Theorem 3.5. *Let the assumptions of Theorem 3.3 hold and define the quantities (see (2.4))*

$$a_{1,n}(V) = \sum_{j=1}^{n} \measuredangle(\Phi(j-1,0)V, \Phi(j,0)V) \quad n \in \mathbb{N},\ V \in \mathcal{G}(s,d).$$

Then the following holds for all $V \in \mathcal{G}(s,d)$

$$\limsup_{n\to\infty} \frac{1}{n} a_{1,n}(V) = \limsup_{n\to\infty} \frac{1}{n} a_{1,n}(\mathcal{T}_0(V)), \tag{3.23}$$

and similarly with $\liminf$ *instead of* $\limsup$. *The outer angular values satisfy*

$$\hat{\theta}_s = \sup_{V\in\mathcal{D}_0(s,d)} \limsup_{n\to\infty} \frac{1}{n} a_{1,n}(V), \quad \underset{\wedge}{\theta}_s = \sup_{V\in\mathcal{D}_0(s,d)} \liminf_{n\to\infty} \frac{1}{n} a_{1,n}(V). \tag{3.24}$$

If $\dim(\mathcal{W}^i_m) = 1$ *for all* $i = 1, \dots, d$ *and* $m \in \mathbb{N}_0$, *then the first lower and upper outer angular values have the form*

$$\begin{aligned}\underset{\wedge}{\theta}_1 &= \max_{i=1,\dots,d} \liminf_{n\to\infty} \frac{1}{n} \sum_{j=1}^{n} \measuredangle(\mathcal{W}^i_{j-1}, \mathcal{W}^i_j), \\ \hat{\theta}_1 &= \max_{i=1,\dots,d} \limsup_{n\to\infty} \frac{1}{n} \sum_{j=1}^{n} \measuredangle(\mathcal{W}^i_{j-1}, \mathcal{W}^i_j).\end{aligned} \tag{3.25}$$

Proof. From the triangle inequality (Proposition 2.2) we obtain

$$\begin{aligned}|a_{1,n}(V) - a_{1,n}(\mathcal{T}_0(V))| &\leq \sum_{j=1}^{n} \{\measuredangle(\Phi(j-1,0)V, \Phi(j-1,0)\mathcal{T}_0(V)) \\ &+ \measuredangle(\Phi(j,0)V, \Phi(j,0)\mathcal{T}_0(V))\} \leq 2\sum_{j=0}^{n} \measuredangle(\Phi(j,0)V, \Phi(j,0)\mathcal{T}_0(V)).\end{aligned} \tag{3.26}$$

Theorem 3.3 shows that the angles decay geometrically for $j \geq \bar{j}(0,V)$, hence the right-hand side is uniformly bounded by a constant depending on V only. Therefore (3.23) follows, and (3.24) is an immediate consequence by taking the supremum with respect to V.

In case $s = 1$ and $\dim(\mathcal{W}_m^i) = 1$ for $i = 1, \dots, d$ the set $\mathcal{D}_0(1,d) = \{\mathcal{W}_0^i : i = 1, \dots, d\}$ becomes finite. Moreover, we have $\Phi(j,0)\mathcal{W}_0^i = \mathcal{W}_j^i$ by the invariance condition (3.6). Thus, the formula (3.24) simplifies to (3.25). ∎

In view of Theorem 3.3, we revisit crucial examples from [6, Section 3.2]. The first model is defined for $n \in \mathbb{N}_0$ and $0 \leq \varphi_0 < \varphi_1 \leq \frac{\pi}{2}$ by

$$A_n = \begin{cases} \begin{pmatrix} \cos(\varphi_0) & -\sin(\varphi_0) \\ \sin(\varphi_0) & \cos(\varphi_0) \end{pmatrix}, & \text{for } n = 0 \vee n \in \bigcup_{\ell=1}^{\infty} [2^{2\ell-1}, 2^{2\ell} - 1] \cap \mathbb{N}, \\ \begin{pmatrix} \cos(\varphi_1) & -\sin(\varphi_1) \\ \sin(\varphi_1) & \cos(\varphi_1) \end{pmatrix}, & \text{otherwise.} \end{cases}$$

For this example, upper and lower angular values do not coincide in general, more precisely, the diagram (2.7) now reads

$$\begin{array}{ccccccc} \underset{\wedge}{\theta}_{[1]} & < & \underset{\wedge}{\theta}_1 & < & \hat{\theta}_1 & < & \hat{\theta}_{[1]} \\ \| & & \| & & \| & & \| \\ \underline{\theta}_{[1]} & < & \underline{\theta}_1 & < & \bar{\theta}_1 & < & \bar{\theta}_{[1]}. \end{array}$$

For the second example, defined for $n \in \mathbb{N}_0$ by

$$A_n := \begin{cases} \begin{pmatrix} -1 & 0 \\ 0 & 1 \end{pmatrix}, & \text{for } n \in \bigcup_{\ell=1}^{\infty} [2 \cdot 2^{\ell} - 4, 3 \cdot 2^{\ell} - 5], \\ \begin{pmatrix} 1 & 0 \\ 0 & \frac{1}{2} \end{pmatrix}, & \text{otherwise} \end{cases}$$

inner and outer angular values differ, i.e. the diagram (2.7) turns into

$$\begin{array}{ccccccc} \underset{\wedge}{\theta}_{[1]} & = & \underset{\wedge}{\theta}_1 & = & \hat{\theta}_1 & = & \hat{\theta}_{[1]} \\ \| & & \wedge & & \wedge & & \wedge \\ \underline{\theta}_{[1]} & < & \underline{\theta}_1 & < & \bar{\theta}_1 & < & \bar{\theta}_{[1]}. \end{array}$$

The dichotomy spectrum of the first example is given by $\Sigma_{\mathrm{ED}} = \{1\}$ and for the second example, we obtain $\Sigma_{\mathrm{ED}} = [\frac{1}{2}, 1]$. In both cases $\mathcal{W}_k^1 = \mathbb{R}^2$ for all $k \in \mathbb{N}$. Thus one-dimensional trace spaces agree with the given space. In particular, the detection of angular values cannot be reduced by Theorem 3.3 and Theorem 3.5 to lower dimensional spaces.

3.3. Inner angular values and spectral bundles. Inner angular values are more difficult to handle, both numerically and theoretically, since the supremum over all subspaces is taken before going to the limit. For general dimensions we do not have a result comparable to Theorem 3.3. However, for one-dimensional subspaces a reduction is possible under a uniformity condition. Recall from (2.4) the notion

$$a_{m,n}(v) = \sum_{j=m}^{n} \measuredangle(\Phi(j-1,0)v, \Phi(j,0)v) \quad m,n \in \mathbb{N},\ v \in \mathbb{R}^d, v \neq 0 \tag{3.27}$$

with $a_{m,n}(v) = 0$ for $m > n$. For a subspace $V \subseteq \mathbb{R}^d$ we introduce the quantity

$$\bar{\theta}_1(V) = \limsup_{n\to\infty} \sup_{v \in V, v \neq 0} \frac{a_{1,n}(v)}{n}.$$

Theorem 3.6. *Let the assumptions of Theorem 3.3 hold. Further assume that the inner and the uniform inner angular values (cf. (2.5), (2.6) and (2.7)) agree within each fiber, i.e. for $i = 1, \dots, \ell$ the following holds*

$$\overline{\theta}_1(\mathcal{W}_0^i) = \lim_{n\to\infty} \frac{1}{n} \sup_{v\in\mathcal{W}_0^i, v\neq 0} \sup_{k\in\mathbb{N}_0} a_{k+1,k+n}(v). \tag{3.28}$$

Then the first inner angular value $\overline{\theta}_1(\mathbb{R}^d)$ satisfies

$$\overline{\theta}_1(\mathbb{R}^d) = \max_{i=1,\dots,\ell} \overline{\theta}_1(\mathcal{W}_0^i).$$

Proof. The main step is to show for $i = 1, \dots, \ell$

$$\overline{\theta}_1(\mathcal{R}(P_{0,i}^s)) \le \max\left(\overline{\theta}_1(\mathcal{W}_0^i), \overline{\theta}_1(\mathcal{R}(P_{0,i+1}^s))\right). \tag{3.29}$$

Since $P_{0,1}^s = I_d$, $P_{0,\ell+1}^s = 0$ and $\sup_\emptyset = 0$, we obtain by induction

$$\overline{\theta}_1(\mathbb{R}^d) \le \max_{i=1,\dots,\ell} \overline{\theta}_1(\mathcal{W}_0^i).$$

The converse inequality "$\ge$" is obvious, hence our assertion is proved.

In the following we choose $j_\star$ such that (cf. (3.19))

$$2K^2 q^{j_\star} \le 1, \quad \text{where} \quad q := \max_{i=1,\dots,\ell} \frac{\sigma_{i+1}^+}{\sigma_i^-} < 1.$$

For the proof of (3.29) it is enough to consider $v \in \mathcal{R}(P_{0,i}^s)$ with $v \notin \mathcal{R}(P_{0,i+1}^s)$ and $v \notin \mathcal{W}_0^i$. Figure 3.5 illustrates the idea of this proof. We choose $\gamma \in R_{i+1}$ and apply

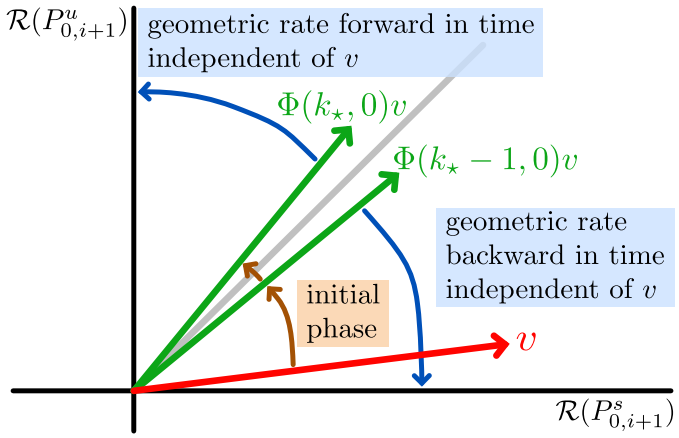

Figure 3.5: Idea of proof for Theorem 3.6. First, we construct a v-dependent index $k_\star$, such that $\Phi(k_\star, 0)v$ is just above the diagonal. Then, we exploit geometric convergence forward resp. backward in time for proving v-independent estimates.

Theorem 3.2 to Φ_γ and $V = \operatorname{span}(v)$ as in Step 2 of the proof of Theorem 3.3. Note that the projector $Q_{0,i+1}^s : V \to \mathcal{R}(P_{0,i+1}^s) \cap V$ from (3.15) is trivial since V is one-dimensional

and $v \notin \mathcal{R}(P^s_{0,i+1})$. Moreover, by (3.5) we have $\mathcal{P}_{0,i}v = P^u_{0,i+1}P^s_{0,i}v = P^u_{0,i+1}v \neq 0$. Therefore, we can invoke inequality (3.11) from the proof of Theorem 3.2 with $\tilde{P} = P^u_{k,i+1}$, $\rho^s_k(v) = \frac{\|P^s_{0,i+1}v\|}{\|P^u_{0,i+1}v\|}$, $\alpha_s\alpha_u \leq q$. This shows

$$\|P^s_{k,i+1}\Phi_\gamma(k,0)v\| \leq K^2 q^k \rho^s_k(v)\|P^u_{k,i+1}\Phi_\gamma(k,0)v\| \quad \forall k \in \mathbb{N}_0.$$

We conclude that the following index, depending on v, exists

$$k_\star = k_\star(v) = \min\{k \in \mathbb{N}_0 : \|P^s_{k,i+1}\Phi_\gamma(k,0)v\| \leq \|P^u_{k,i+1}\Phi_\gamma(k,0)v\|\}.$$

Applying Theorem 3.2 once more to Φ_γ and $V = \operatorname{span}(\Phi_\gamma(k_\star,0)v)$ then shows for $j \geq k_\star + j_\star$

$$\begin{aligned}&\measuredangle(\Phi(j,k_\star)\Phi(k_\star,0)v, \Phi(j,k_\star)P^u_{k_\star,i+1}\Phi(k_\star,0)v)\\ &= \measuredangle(\Phi(j,0)v, \Phi(j,0)P^u_{0,i+1}v) \leq \frac{2K^2}{\sqrt{3}}q^{j-k_\star}.\end{aligned}$$

Next we estimate angles for $j \leq k_\star$ by invoking (3.14) with $k = k_\star - 1$ and $V = \operatorname{span}(\Phi_\gamma(k_\star - 1, 0)v)$. Since $v \notin \mathcal{W}^i_0$ the projector in (3.12) is trivial, and (3.13) holds by the choice of $j_\star$. Hence we obtain for $0 \leq j \leq k_\star - 1 - j_\star$

$$\begin{aligned}&\measuredangle(\Phi(j,k_\star-1)\Phi(k_\star-1,0)v, \Phi(j,k_\star)P^s_{k_\star,i+1}\Phi(k_\star,0)v)\\ &= \measuredangle(\Phi(j,0)v, \Phi(j,0)P^s_{0,i+1}v) \leq \frac{2K^2}{\sqrt{3}}q^{k_\star-1-j}.\end{aligned}$$

Combining these estimates with the triangle inequality we find with suitable constants C independent of n, j, v,

$$\begin{aligned}\frac{a_{1,n}(v)}{n} &= \frac{1}{n}\sum_{j=1}^{n}\measuredangle(\Phi(j-1,0)v, \Phi(j,0)v)\\ &\leq \frac{1}{n}\Big[\Big\{\sum_{j=1}^{k_\star-1-j_\star} + \sum_{j=k_\star+1+j_\star}^{n}\Big\}\measuredangle(\Phi(j-1,0)v, \Phi(j,0)v) + (2j_\star+1)\frac{\pi}{2}\Big]\\ &\leq \frac{1}{n}\Big[\frac{4K^2}{\sqrt{3}}\Big(\sum_{j=0}^{k_\star-1-j_\star} q^{k_\star-1-j} + \sum_{j=k_\star}^{n} q^{j-k_\star}\Big) + C\\ &\quad + \sum_{j=1}^{k_\star}\measuredangle(\Phi(j-1,0)P^s_{0,i+1}v, \Phi(j,0)P^s_{0,i+1}v)\\ &\quad + \sum_{j=k_\star+1}^{n}\measuredangle(\Phi(j-1,0)P^u_{0,i+1}v, \Phi(j,0)P^u_{0,i+1}v)\Big]\\ &\leq \frac{1}{n}\left[C + a_{1,k_\star}(P^s_{0,i+1}v) + a_{k_\star+1,n}(P^u_{0,i+1}v)\right].\end{aligned} \tag{3.30}$$

Given $\varepsilon > 0$, assumption (3.28) yields a number $n_0 = n_0(\varepsilon)$ such that

$$\begin{aligned} \frac{1}{n} \sup_{k\in\mathbb{N}_0} \sup_{v\in\mathcal{W}_0^i} a_{k+1,k+n}(v) &\le \overline{\theta}_1(\mathcal{W}_0^i) + \varepsilon, \quad \forall n \ge n_0, \\ \frac{1}{n} \sup_{v\in\mathcal{R}(P^s_{0,i+1})} a_{1,n}(v) &\le \overline{\theta}_1(\mathcal{R}(P^s_{0,i+1})) + \varepsilon, \quad \forall n \ge n_0. \end{aligned} \tag{3.31}$$

Thus we have

$$\begin{aligned} a_{k_\star+1,n}(P^u_{0,i+1}v) &\le \begin{cases} (n-k_\star)(\overline{\theta}_1(\mathcal{W}_0^i)+\varepsilon), & \text{if } n-k_\star \ge n_0, \\ n_0\tfrac{\pi}{2}, & \text{if } n-k_\star < n_0, \end{cases} \\ a_{1,k_\star}(P^s_{0,i+1}v) &\le \begin{cases} k_\star(\overline{\theta}_1(\mathcal{R}(P^s_{0,i+1}))+\varepsilon), & \text{if } k_\star \ge n_0, \\ n_0\tfrac{\pi}{2}, & \text{if } k_\star < n_0. \end{cases} \end{aligned}$$

Summing up, we obtain for $n \ge n_0(\varepsilon)$,

$$\begin{aligned} \frac{a_{1,n}(v)}{n} \le \frac{1}{n}\big[&\min(k_\star,n)(\overline{\theta}_1(\mathcal{R}(P^s_{0,i+1}))+\varepsilon) + (n-\min(n,k_\star))(\overline{\theta}_1(\mathcal{W}_0^i)+\varepsilon) \\ &+C + n_0\pi\big] \le \max(\overline{\theta}_1(\mathcal{W}_0^i), \overline{\theta}_1(\mathcal{R}(P^s_{0,i+1}))) + \varepsilon + \frac{1}{n}(C+n_0\pi). \end{aligned}$$

Finally, the assertion (3.29) follows by taking the supremum over v and making the last term small for n sufficiently large. ∎

3.4. Uniform angular values and spectral bundles. In this section we extend Theorem 3.5 and Theorem 3.6 to uniform outer and inner angular values. As before, we show that it is enough to compute angular values for subspaces which have their basis in the fibers induced by the dichotomy spectrum.

Theorem 3.7. *Let the assumptions of Theorem 3.3 hold. Then the uniform outer angular values $\hat{\theta}_{[s]}, \underset{\wedge}{\theta}_{[s]}$, $s = 1, \dots, d$, can be represented with the partial sums (2.4) and the trace space (3.18) as follows:*

$$\hat{\theta}_{[s]} = \sup_{V\in\mathcal{D}_0(s,d)} \lim_{n\to\infty} \sup_{k\in\mathbb{N}_0} \frac{1}{n} a_{k+1,k+n}(V), \tag{3.32}$$

$$\underset{\wedge}{\theta}_{[s]} = \sup_{V\in\mathcal{D}_0(s,d)} \lim_{n\to\infty} \inf_{k\in\mathbb{N}_0} \frac{1}{n} a_{k+1,k+n}(V). \tag{3.33}$$

With the partial sums from (3.27), the first uniform inner angular value satisfies

$$\overline{\theta}_{[1]} = \max_{i=1,\dots,\ell} \overline{\theta}_{[1]}(\mathcal{W}_0^i), \quad \text{where} \quad \overline{\theta}_{[1]}(V) = \lim_{n\to\infty} \sup_{v\in V} \sup_{k\in\mathbb{N}_0} \frac{1}{n} a_{k+1,k+n}(v). \tag{3.34}$$

Proof. Recall $a_{m,n}(V)$ from (2.4) and use (3.26), (3.19) to find that $V \in \mathcal{G}(s,d)$ satisfies with some constant C depending on V but not on k, n,

$$\begin{aligned} |a_{k+1,k+n}(V) - a_{k+1,k+n}(\mathcal{T}_0(V))| &\le 2\sum_{j=k}^{k+n} \measuredangle(\Phi(j,0)V, \Phi(j,0)(\mathcal{T}_0(V))) \\ &\le 2C(0,V)\sum_{j=k}^{k+n} q^{j-k} \le C. \end{aligned} \tag{3.35}$$

Given $\varepsilon > 0$, choose n_0 such that for $n \geq n_0$

$$\Big|\frac{1}{n}\sup_{k\in\mathbb{N}_0} a_{k+1,k+n}(V) - \lim_{m\to\infty}\frac{1}{m}\sup_{k\in\mathbb{N}_0} a_{k+1,k+m}(V)\Big| \leq \varepsilon.$$

Then select $k(n) \in \mathbb{N}_0$ such that $\frac{1}{n}|a_{k(n)+1,k(n)+n}(V) - \sup_{k\in\mathbb{N}_0} a_{k+1,k+n}(V)| \leq \varepsilon$ holds for $n \geq n_0$. This implies

$$\Big|\frac{1}{n}a_{k(n)+1,k(n)+n}(V) - \lim_{m\to\infty}\frac{1}{m}\sup_{k\in\mathbb{N}_0} a_{k+1,k+m}(V)\Big| \leq 2\varepsilon, \quad n \geq n_0.$$

With (3.35) we obtain for $n \geq n_0$

$$\begin{aligned}\lim_{m\to\infty}\frac{1}{m}\sup_{k\in\mathbb{N}_0} a_{k+1,k+m}(V) &\leq \frac{1}{n}a_{k(n)+1,k(n)+n}(V) + 2\varepsilon\\ &\leq \frac{C}{n} + \frac{1}{n}a_{k(n)+1,k(n)+n}(\mathcal{T}_0(V)) + 2\varepsilon\\ &\leq \frac{C}{n} + \frac{1}{n}\sup_{k\in\mathbb{N}_0} a_{k+1,k+n}(\mathcal{T}_0(V)) + 2\varepsilon.\end{aligned}$$

As $n \to \infty$ this shows

$$\lim_{n\to\infty}\frac{1}{n}\sup_{k\in\mathbb{N}_0} a_{k+1,k+n}(V) \leq 2\varepsilon + \lim_{n\to\infty}\frac{1}{n}\sup_{k\in\mathbb{N}_0} a_{k+1,k+n}(\mathcal{T}_0(V)).$$

A corresponding inequality with V and $\mathcal{T}_0(V)$ exchanged, is proved in the same manner, and (3.32) follows by taking the supremum over $V \in \mathcal{G}(s,d)$. The same type of estimate leads to (3.33). The formula in (3.34) follows by adapting the proof of Theorem 3.6. For the quantities $\overline{\theta}_{[1]}(V)$ from (3.34) we show

$$\overline{\theta}_{[1]}(\mathcal{R}(P^s_{0,i})) \leq \max\left(\overline{\theta}_{[1]}(\mathcal{W}^i_0), \overline{\theta}_{[1]}(\mathcal{R}(P^s_{0,i+1}))\right), \quad i = 1,\dots,\ell. \tag{3.36}$$

The estimate (3.30) for $v \in \mathcal{R}(P^s_{0,i}) \setminus (\mathcal{R}(P^s_{0,i+1}) \cup \mathcal{W}^i_0)$ now reads

$$\frac{1}{n}a_{k+1,k+n}(v) \leq \frac{1}{n}\left[C + a_{k+1,k_\star-j_\star-1}(P^s_{0,i+1}v) + a_{\max(k,k_\star+j_\star+1),n+k}(P^u_{0,i+1}v)\right].$$

Recall $a_{m,n} = 0$ for $m > n$ and note that there is no relation between $k, k_\star(v)$ and n. The condition (3.31) for n_0 turns into

$$\begin{aligned}\frac{1}{n}\sup_{v\in\mathcal{W}^i_0}\sup_{k\in\mathbb{N}_0} a_{k+1,k+n}(v) &\leq \overline{\theta}_{[1]}(\mathcal{W}^i_0) + \varepsilon, \quad \forall n \geq n_0,\\ \frac{1}{n}\sup_{v\in\mathcal{R}(P^s_{0,i+1})}\sup_{k\in\mathbb{N}_0} a_{k+1,k+n}(v) &\leq \overline{\theta}_{[1]}(\mathcal{R}(P^s_{0,i+1})) + \varepsilon, \quad \forall n \geq n_0.\end{aligned}$$

This leads to

$$\begin{aligned}a_{k_1,n+k}(P^u_{0,i+1}v) &\leq \begin{cases}(n+k-k_1)(\overline{\theta}_{[1]}(\mathcal{W}^i_0)+\varepsilon), & \text{if } n+k-k_1 \geq n_0,\\ n_0\tfrac{\pi}{2}, & \text{if } n+k-k_1 < n_0,\end{cases}\\ a_{k+1,k_2}(P^s_{0,i+1}v) &\leq \begin{cases}(k_2-k-1)(\overline{\theta}_{[1]}(\mathcal{R}(P^s_{0,i+1}))+\varepsilon), & \text{if } k_2-k-1 \geq n_0,\\ n_0\tfrac{\pi}{2}, & \text{if } k_2-k-1 < n_0,\end{cases}\end{aligned} \tag{3.37}$$

where $k_1 = \max(k, k_\star + j_\star + 1)$, $k_2 = k_\star - j_\star - 1$. In both cases $k \geq k_\star + j_\star + 1$ and $k < k_\star + j_\star + 1$ we find the estimate $n + k - k_1 + k_2 - k - 1 \leq n$ for the sum of coefficients in (3.37). Hence, we can continue

$$\frac{1}{n} a_{k+1,k+n}(v) \leq \frac{1}{n} \left[C + n_0 \pi + n \left(\max(\overline{\theta}_{[1]}(\mathcal{W}_0^i), \overline{\theta}_{[1]}(\mathcal{R}(P^s_{0,i+1}))) + \varepsilon \right) \right].$$

Taking the supremum over k and v and then letting $n \to \infty$ yields the assertion (3.36) as in the proof of Theorem 3.6. ∎

4. Numerical algorithms and results. The aim of this section is to develop an algorithm for the numerical detection of outer angular values. The previous section provides the essential reduction result in Theorem 3.5:

$$\begin{aligned} \hat{\theta}_s &= \sup_{V \in \mathcal{G}(s,d)} \limsup_{n \to \infty} \frac{1}{n} \sum_{j=1}^{n} \measuredangle(\Phi(j-1,0)V, \Phi(j,0)V) \\ &= \sup_{V \in \mathcal{D}_0(s,d)} \limsup_{n \to \infty} \frac{1}{n} \sum_{j=1}^{n} \measuredangle(\Phi(j-1,0)V, \Phi(j,0)V). \end{aligned}$$

The search for the supremum of V in $\mathcal{D}_0(s,d)$ instead of $\mathcal{G}(s,d)$ reduces the computational effort substantially and, in some cases, one needs to consider only finitely many subspaces.

This observation also illuminates the fact, that various numerical approaches tend to fail:

- Algorithms that are based on a simple forward iteration cannot provide the largest angular value. A generic subspace is pushed by the dynamics towards the most unstable trace space of equal dimension, see the upper row in Figure 3.4. But in general, the angular value is not attained in this subspace. For finding the correct angular value, also non-generic subspaces must be considered, as sketched in the lower row of Figure 3.4.
- Algorithms that are based on the computation of eigenvalues and eigenspaces, e.g. by applying the Schur decomposition, provide good results for autonomous systems. This fits well to our theory, since in the autonomous case, spectral bundles w.r.t. the dichotomy spectrum are indeed eigenspaces. The corresponding analysis for autonomous systems is carried out in detail in [6]. Further note that for nonautonomous modes, eigenvalues are dynamically irrelevant, which has first been shown by Vinograd, see [28]. Corresponding algorithms fail in testing all trace subspaces.

To circumvent these issues, we first detect the dichotomy spectrum and the corresponding spectral bundles. Then all trace subspaces become available, resulting in a numerically expensive but reliable approximation of $\hat{\theta}_s$.

4.1. An algorithm for computing angular values. Based on the results from Section 3, we propose the following three steps for the numerical approximation of $\hat{\theta}_s$.

Step 1: Computation of the dichotomy spectrum. The computation of Bohl exponents leads to an efficient algorithm for the approximation of the dichotomy spectrum. Upper and lower Bohl exponents of the scalar difference equation

$$u_{n+1} = a_n u_n, \quad n \in \mathbb{I}, \quad 0 < \inf_{n \in \mathbb{I}} |a_n| \leq \sup_{n \in \mathbb{I}} |a_n| < \infty$$

are defined as, see [20]

$$\underline{\beta}(a_{\mathbb{I}}) := \lim_{n\to\infty} \inf_{\kappa\in\mathbb{I}} \left(\prod_{j=\kappa}^{\kappa+n-1} |a_j| \right)^{\frac{1}{n}}, \qquad \overline{\beta}(a_{\mathbb{I}}) := \lim_{n\to\infty} \sup_{\kappa\in\mathbb{I}} \left(\prod_{j=\kappa}^{\kappa+n-1} |a_j| \right)^{\frac{1}{n}}.$$

It follows that $\Sigma_{\mathrm{ED}} = [\underline{\beta}(a_{\mathbb{I}}), \overline{\beta}(a_{\mathbb{I}})]$.

For the d-dimensional difference equation (1.1), a corresponding result is more delicate to obtain. One may first transform the system into upper triangular form, using a `qr`-decomposition $A = QT$ of a given matrix A into the product of an orthogonal matrix Q and an upper triangular matrix T, see [18, Section 4.4] and [11]:

$$\begin{aligned} &Q_0 T_0 = \mathtt{qr}(A_0) \\ &\textbf{for } j = 1, 2, \dots \textbf{ do} \\ &\quad Q_j T_j = \mathtt{qr}(A_j Q_{j-1}) \\ &\textbf{end for} \end{aligned}$$

Note that $A_j = Q_j T_j Q_{j-1}^{\top}$ for $j \geq 1$. For non-degenerate models, the Bohl exponents of the diagonal entries of T_j (denoted by $T_j(i,i)$) determine the dichotomy spectrum, cf. [26] for more details on the theoretical background. Fix $H \in \mathbb{N}$ sufficiently large, compute

$$\beta(i,\kappa) := \left(\prod_{j=\kappa}^{\kappa+H} |T_j(i,i)| \right)^{\frac{1}{H}}, \quad i = 1, \dots, d, \quad \kappa = 0, 1, \dots \tag{4.1}$$

and obtain with $\underline{\beta}(i) := \min_\kappa \beta(i,\kappa)$, $\overline{\beta}(i) := \max_\kappa \beta(i,\kappa)$ the approximate spectrum $\Sigma_{\mathrm{ED}} \approx \bigcup_{i=1}^{d} [\underline{\beta}(i), \overline{\beta}(i)]$.

Step 2: Computation of spectral bundles. Recall for $k \in \mathbb{N}$ and $i \in \{1, \dots, \ell\}$ the representation (3.3), (3.5) of the spectral bundle $\mathcal{W}_k^i = \mathcal{R}(\mathcal{P}_{k,i}) = \mathcal{R}(P_{k,i}^s P_{k,i+1}^u)$ with $\dim(\mathcal{W}_k^i) = d_i$. For computing these sets numerically, we apply the ansatz, proposed in [19, Section 2.5]. Take d_i random vectors $r_\nu \in \mathbb{R}^d$ and obtain a basis of $\mathcal{W}_k^i$ (in a generic sense) by calculating $\mathcal{P}_{k,i} r_\nu$ for $\nu = 1, \dots, d_i$. For this task, we choose $\gamma_i \in R_i$, $\gamma_{i+1} \in R_{i+1}$, $0 \leq n_- \ll k \ll n_+$ and solve for each $\nu \in \{1, \dots, d_i\}$ and $n \in \{n_-, \dots, n_+ - 1\}$ the inhomogeneous linear systems

$$v_{n+1}^\nu = \frac{1}{\gamma_{i+1}} A_n v_n^\nu + \delta_{n,k-1} r_\nu, \quad u_{n+1}^\nu = \frac{1}{\gamma_i} A_n u_n^\nu - \delta_{n,k-1} A_{k-1} v_{k-1}^\nu \tag{4.2}$$

in a least squares sense. Here, δ denotes the Kronecker symbol. For the solutions of (4.2) one has $\mathcal{P}_{k,i} r_\nu \approx u_k^\nu$, and we refer to [19, Section 2.6] for precise error estimates.

Step 3: Computation of angular values. Assume that the spectral bundles $\mathcal{W}_j^i$, $i = 1, \dots, \ell$, $j = k, \dots, k+m$ have been computed in step 2 for a fixed value of $k \in \mathbb{N}$ and for an interval of fixed length $m \in \mathbb{N}$. We present a numerical scheme for computing approximate values of $\hat{\theta}_s$ in case $s \in \{1, 2\}$. Assume that $\dim(\mathcal{W}_k^i) \in \{1, 2\}$ and introduce the balls $\mathcal{B}_k^i = \{v \in \mathcal{W}_k^i : \|v\| = 1\}$ for all $i \in \{1, \dots, \ell\}$. For a subspace $V \in \mathcal{G}(s, d)$ (respectively a vector $v \in \mathbb{R}^d$) we abbreviate (cf. (2.4))

$$\theta_s(V) = \frac{1}{n} a_{k+1,k+n}(V) = \frac{1}{n} \sum_{j=k+1}^{k+n} \measuredangle(\Phi(j-1,k)V, \Phi(j,k)V).$$

Starting with $s = 1$ our scheme reads:

for $i = 1, \dots, \ell$ **do**
  $w^i = \max_{v \in \mathcal{B}_k^i} \theta_1(v)$
end for
$\hat{\theta}_1 = \max_{i=1,\dots,\ell} w^i$.

If $\dim(\mathcal{W}_k^i) = 1$ then $\theta_1(\mathcal{W}_k^i)$ is computed for a single one-dimensional subspace. The detection of $\max_{v \in \mathcal{B}_k^i} \theta_1(v)$ is a one-dimensional optimization problem if $\dim \mathcal{W}_k^i = 2$. For this task, we apply the MATLAB-routine `fminbnd` that is based on golden section search and parabolic interpolation.

The corresponding scheme for $s = 2$ is given by:

$\kappa = 0$
for $i = 1, \dots, \ell$ **do**
  if $\dim(\mathcal{W}_k^i) = 2$ **then**
    $\kappa = \kappa + 1$
    $w^\kappa = \theta_2(\mathcal{W}_k^i)$
  end if
end for
for $i_1 = 1, \dots, \ell - 1$ **do**
  for $i_2 = i_1 + 1, \dots, \ell$ **do**
    $\kappa = \kappa + 1$
    $w^\kappa = \max_{x \in \mathcal{B}_k^{i_1},\, y \in \mathcal{B}_k^{i_2}} \theta_2(\mathrm{span}(x, y))$
  end for
end for
$\hat{\theta}_2 = \max_{i=1,\dots,\kappa} w^i$.

Note that the algorithm avoids to distinguish cases. If $\dim(\mathcal{W}_k^{i_1}) = \dim(\mathcal{W}_k^{i_2}) = 1$ then $\theta_2(\mathcal{W}_k^{i_1} \oplus \mathcal{W}_k^{i_2})$ is computed for a single two-dimensional subspace. In case $\dim(\mathcal{W}_k^{i_1}) + \dim(\mathcal{W}_k^{i_2}) = 3$, we solve a one-dimensional optimization problem with the tools, described in case $s = 1$. If $\dim(\mathcal{W}_k^{i_1}) + \dim(\mathcal{W}_k^{i_2}) = 4$ then the optimization problem is two-dimensional, and we apply the MATLAB-command `fminsearch`, which uses a derivative-free method for finding minima of unconstrained multivariable functions.

In all cases, we avoid numerical errors during the iteration of $\Phi(j, k)x$ for $x \in \mathcal{W}_k^i$ (i.e. convergence towards the most unstable direction) by renormalizing the resulting output to $\mathcal{W}_j^i$ after each step.

Details for step 1. Let a sequence of matrices $(A_j)_{j=0,\dots,M-1}$ be given, where $M = 100\mu$, $\mu \in \mathbb{N}$, $\mu \geq 2$. For computing the Bohl exponents in (4.1), we choose $H = \frac{M}{2}$. We sort the Bohl exponents such that $\underline{\beta}(1) \geq \dots \geq \underline{\beta}(d)$. In step 2, a sufficiently large gap is needed for detecting spectral bundles accurately. Therefore, we join two spectral intervals $[\underline{\beta}(i+1), \overline{\beta}(i+1)]$ and $[\underline{\beta}(i), \overline{\beta}(i)]$ into $[\underline{\beta}(i+1), \overline{\beta}(i)]$ if the condition $\overline{\beta}(i+1) + 0.1 \geq \underline{\beta}(i)$ holds for $i \in \{1, \dots, d-1\}$. One the one hand, we lose information about the corresponding trace spaces in the vanishing resolvent interval but on the other hand we improve numerical stability. Note that the information lost can be recovered in step 3, by solving an optimization problem.

Details for step 2. Choose $n_- = 0$ and $n_+ = M$. For getting accurate numerical data, we define a gap-size of length 50 and ensure this gap between k and both sides $n_\pm$ of the

finite interval. Then, the least squares solution of (4.2) is simultaneously computed for all $k \in \mathbb{I} = [50, M-50] \cap \mathbb{Z}$. One may avoid large least squares problems by subdividing the system into small problems on subintervals of length 200. In this way, we obtain bases of $\mathcal{W}_k^i$ for $k \in \mathbb{I}$ and $i \in \{1, \dots, \ell\}$. If these fiber bundles are two-dimensional, we choose an orthonormal basis at each time instance.

Details for step 3. This step relies on the fibers which have been computed in step 2 for $k \in \mathbb{I}$. Thus, we start the algorithm in step 3 with the settings $k = 50$ and $m = M-100$.

4.2. Numerical experiments. We apply our algorithm from Section 4.1 to several models. First we reconsider some autonomous difference equations from cf. [6]. For this class of systems the algorithm from [6, Section 6] uses a series of Schur decompositions and one-dimensional optimization if necessary. Although this is more efficient for autonomous systems, we still apply in the following our general algorithm to the autonomous case in order to illustrate its performance. Furthermore, we apply both algorithms in Section 4.2.2 to autonomous systems and compare the results.

4.2.1. Two-dimensional models. We begin with several two-dimensional models for which angular values are analytically known. For these examples we always find point spectrum which we approximate by upper and lower Bohl exponents. In some cases upper and lower exponents coincide up to machine accuracy, while in other models, we numerically observe intervals of length $\approx 10^{-3}$. In the following we denote by $T_\varphi = \left(\begin{smallmatrix} \cos\varphi & -\sin\varphi \\ \sin\varphi & \cos\varphi \end{smallmatrix}\right)$ a rotation matrix.

A_n	spectral intervals	$\hat{\theta}_{1,\text{num}}$	$\lvert\hat{\theta}_1 - \hat{\theta}_{1,\text{num}}\rvert$
$\left(\begin{smallmatrix} 2 & 0 \\ 0 & 3 \end{smallmatrix}\right)$	$\mathcal{I}_1 = [3,3]$ $\mathcal{I}_2 = [2,2]$	$5 \cdot 10^{-15}$	$5 \cdot 10^{-15}$
$\left(\begin{smallmatrix} \cos\varphi & \sin\varphi \\ \sin\varphi & -\cos\varphi \end{smallmatrix}\right)$	$\mathcal{I}_1 = [1,1]$	$\frac{\pi}{2} - 3{\cdot}10^{-5}$	$3 \cdot 10^{-5}$
$T_{(n+1)\varphi} \cdot \left(\begin{smallmatrix} 2 & 0 \\ 0 & 3 \end{smallmatrix}\right) \cdot T_{-n\cdot\varphi}$	$\mathcal{I}_1 = [2.996, 3.000]$ $\mathcal{I}_2 = [2.000, 2.002]$	$\frac{1}{3} + 6{\cdot}10^{-13}$	$6 \cdot 10^{-13}$
$T_{n\cdot\varphi}$	$\mathcal{I}_2 = [1,1]$	$\frac{\pi}{4} + 3.1{\cdot}10^{-4}$	$3.1 \cdot 10^{-4}$

Table 4.1: Spectral intervals and the first angular value for five examples. We set $\varphi = \frac{1}{3}$ and use our algorithm with $M = 2000$ iterates.

The models from the first three rows in Table 4.1 are autonomous and we obtain approximately the expected results, see [6]. The second example is a reflection which exhibits the angular value $\hat{\theta}_1 = \frac{\pi}{2}$ with a somewhat smaller error. The third model is constructed via a nonautonomous similarity transformation with rotation matrices, and we obtain the angular value $\hat{\theta}_1 = \varphi = \frac{1}{3}$ with high accuracy. Finally, in the last row of Table 4.1 we consider a rotation by the angle $\varphi = \frac{1}{3}$ which is an irrational multiple of π. The angle $\measuredangle(u, T_{n\cdot\varphi}u)$ is $\frac{\pi}{4}$ on average, in agreement with our numerical experiment.

4.2.2. Two autonomous examples. We apply our algorithm as well as [6, Algorithm 6.2] to autonomous examples and compare the resulting output. For this task we take the

normal form

$$A(\rho,\varphi)=\begin{pmatrix}\cos(\varphi) & -\rho^{-1}\sin(\varphi)\\ \rho\sin(\varphi) & \cos(\varphi)\end{pmatrix},\quad 0<\rho\le 1,\quad 0<\varphi\le\frac{\pi}{2} \tag{4.3}$$

and consider first the matrix $A(\frac{1}{7},\frac{1}{3})$. The autonomous algorithm uses an in-depth analysis of the first angular value of (4.3), given in [6, Theorem 6.1]. The resulting angular value is $\hat\theta_{1,\mathrm{auto}}=0.32106$. In coincidence with this result, the algorithm from Section 4.1 yields the spectral interval $\mathcal{I}_1=[0.9991,1.0009]$ and the angular value $\hat\theta_{1,\mathrm{num}}=0.32175$.

Next, we analyze the four-dimensional matrix

$$A=\begin{pmatrix}A(1,\frac{1}{2}) & I_2\\ 0 & \eta A(\frac{1}{2},1.4)\end{pmatrix}$$

with $\eta=1.2$. The algorithm from Section 4.1 findes the spectral intervals

$$\mathcal{I}_1=[1.1992,1.2008]\quad\text{and}\quad\mathcal{I}_2=[1.0000,1.0000]$$

with corresponding angular values

$$\hat\theta_{1,\mathrm{num}}=\theta_1(\mathcal{W}_k^1)=1.355095\quad\text{and}\quad\theta_2(\mathcal{W}_k^2)=0.500000.$$

This fits well to the results of the autonomous algorithm. The corresponding analysis is presented in [6, Section 6.3.2] and provides the angular value $\hat\theta_{1,\mathrm{auto}}=1.355003$.

4.2.3. Angular values and tangent spaces. For a geometric interpretation of angular values, we start with an invertible discrete time dynamical system which is defined on $\mathbb{Z}$. Let $F_n:\mathbb{R}^d\to\mathbb{R}^d$, $n\in\mathbb{Z}$ be a family of $\mathcal{C}^2$- diffeomorphisms and let

$$x_{n+1}=F_n(x_n),\quad n\in\mathbb{Z}. \tag{4.4}$$

Denote by Ψ the solution operator of (4.4). With respect to a bounded trajectory $\xi_{\mathbb{Z}}:=(\xi_n)_{n\in\mathbb{Z}}$, we introduce the corresponding variational equation

$$u_{n+1}=DF_n(\xi_n)u_n,\quad n\in\mathbb{Z} \tag{4.5}$$

with solution operator Φ. Note that (4.5) has the form (1.1) with $A_n=DF_n(\xi_n)$.

Stable and unstable fiber bundles of $\xi_{\mathbb{Z}}$ are defined at time $\ell\in\mathbb{Z}$ as

$$\mathcal{F}_\ell^s:=\left\{x\in\mathbb{R}^d:\lim_{n\to\infty}|\Psi(n,\ell)(x)-\xi_n|=0\right\},$$
$$\mathcal{F}_\ell^u:=\left\{x\in\mathbb{R}^d:\lim_{n\to-\infty}|\Psi(n,\ell)(x)-\xi_n|=0\right\},$$

and we denote corresponding tangent spaces by $T_{\xi_\ell}\mathcal{F}_\ell^{s,u}$.

We fix $k\in\mathbb{Z}$. For two-dimensional systems with $\dim(\mathcal{F}_\ell^s)=\dim(\mathcal{F}_\ell^u)=1$, we observe that

$$\begin{aligned}\theta_1(\mathcal{W}_k^{2,1})&=\frac{1}{n}\sum_{j=k+1}^{k+n}\measuredangle(\Phi(j-1,k)\mathcal{W}_k^{2,1},\Phi(j,k)\mathcal{W}_k^{2,1})\\&=\frac{1}{n}\sum_{j=k+1}^{k+n}\measuredangle(T_{\xi_{j-1}}\mathcal{F}_{j-1}^{s,u},T_{\xi_j}\mathcal{F}_j^{s,u})\end{aligned}$$

describes the angle between successive stable resp. unstable tangent spaces on average. The maximum of these two averages is $\hat{\theta}_1 = \max\{\theta_1(\mathcal{W}_k^1), \theta_1(\mathcal{W}_k^2)\}$.

In higher dimensional systems, a geometric interpretation of angular values is more involved. If a three-dimensional model, for example, satisfies $\dim(\mathcal{F}_\ell^u) = 1$ and $\dim(\mathcal{F}_\ell^s) = 2$, we get for the one-dimensional unstable direction

$$\theta_1(\mathcal{W}_k^1) = \frac{1}{n} \sum_{j=k+1}^{k+n} \measuredangle(T_{\xi_{j-1}}\mathcal{F}_{j-1}^u, T_{\xi_j}\mathcal{F}_j^u).$$

Next, we consider the two-dimensional stable direction

$$\mathcal{W}_k^s := \begin{cases} \mathcal{W}_k^2, & \text{if } \dim(\mathcal{W}_k^2) = 2, \\ \mathcal{W}_k^2 \oplus \mathcal{W}_k^3, & \text{otherwise.} \end{cases}$$

The first angular value

$$\theta_1(\mathcal{W}_k^s) = \sup_{v \in T_{\xi_k}\mathcal{F}_k^s} \frac{1}{n} \sum_{j=k+1}^{k+n} \measuredangle(\Phi(j-1,k)v, \Phi(j,k)v)$$

describes on average the maximal angle between successive one-dimensional directions in $T_{\xi_\mathbb{Z}}\mathcal{F}_\mathbb{Z}^s$. Combining these result gives $\hat{\theta}_1 = \max\{\theta_1(\mathcal{W}_k^1), \theta_1(\mathcal{W}_k^s)\}$.

For three-dimensional models, also second angular values are of interest. The average angle between successive two-dimensional stable subspaces is given by

$$\theta_2(\mathcal{W}_k^s) = \frac{1}{n} \sum_{j=k+1}^{k+n} \measuredangle(T_{\xi_{j-1}}\mathcal{F}_{j-1}^s, T_{\xi_j}\mathcal{F}_j^s)$$

and the latter formula provides a nice geometrical interpretation. However, for computing $\hat{\theta}_2$, we have to consider further subspaces:

$$\hat{\theta}_2 = \max(\{\theta_2(\mathcal{W}_k^s)\} \cup \{\theta_2(V) : V = \mathcal{W}_k^1 \oplus \operatorname{span}(u) : u \in \mathcal{W}_k^s\}).$$

As a consequence, second and higher anglar values are in general not attained within the stable resp. unstable tangent bundle.

4.2.4. Models of Hénon type. We illustrate the geometric interpretation of angular values from Section 4.2.3 with two autonomous, nonlinear systems. Of interest are the two-dimensional Hénon map [16] as well as its three dimensional variant

$$F^2\begin{pmatrix} x_1 \\ x_2 \end{pmatrix} = \begin{pmatrix} 1 + x_2 - 1.4x_1^2 \\ 0.3x_1 \end{pmatrix}, \quad F^3\begin{pmatrix} x_1 \\ x_2 \\ x_3 \end{pmatrix} = \begin{pmatrix} 1 + x_3 - 1.4x_1^2 \\ x_1 + x_3 \\ 0.2x_1 + 0.1x_2 \end{pmatrix}.$$

The latter model is constructed similar to [7, Example 2], and possesses, like the original Hénon map, a non-trivial attractor.

We choose $M = 2000$, $k = 50$ and compute angular values for the corresponding variational equation (4.5). Note that we apply the algorithm to these models even though we do not know whether the hyperbolicity assumptions are satisfied.

The two-dimensional Hénon model. We choose the initial point close to the Hénon attractor $\xi_0 = \begin{pmatrix} -1.202 & 0.3713 \end{pmatrix}^\top$ and obtain the spectral intervals

$$\mathcal{I}_1 = [1.4896, 1.5481] \quad \text{and} \quad \mathcal{I}_2 = [0.1937, 0.2014]$$

with corresponding angular values

$$\theta_1(\mathcal{W}_k^1) = 0.3644, \quad \theta_1(\mathcal{W}_k^2) = 0.7525.$$

Hence $\hat{\theta}_1 = \theta_1(\mathcal{W}_k^2)$ describes the angle between successive stable tangent spaces on average. Stable and unstable tangent spaces are shown in Figure 4.1. In addition, we present approximations of the stable and of the unstable manifold with respect to the fixed point ξ.

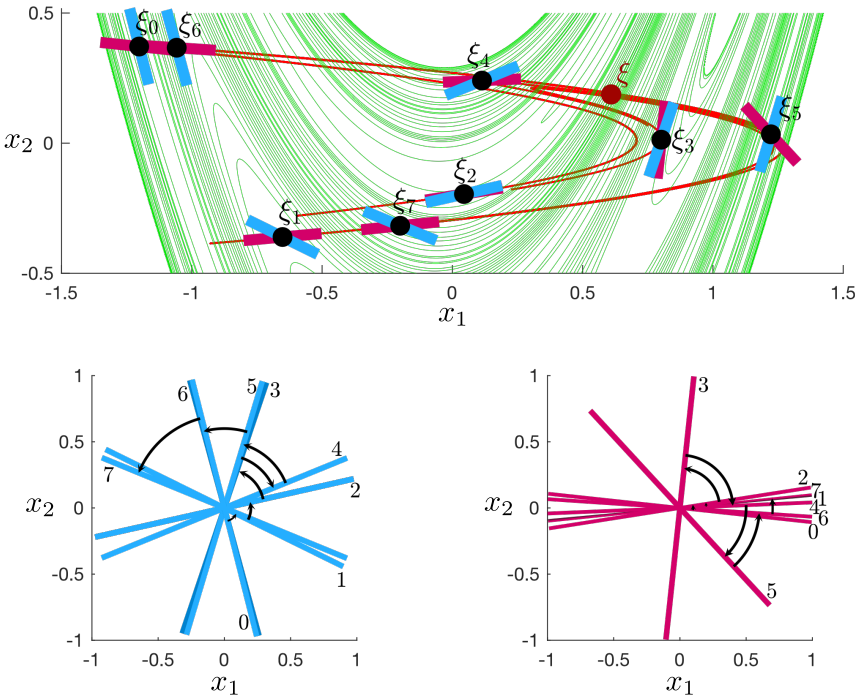

Figure 4.1: Upper panel: Stable (green) and unstable (red) manifolds of the fixed point ξ of the two-dimensional Hénon model. Lower panel: Successive stable (left) and unstable (right) tangent spaces.

Finally, we illustrate the dependence of $\hat{\theta}_1$ on the length m of the finite interval in Figure 4.2.

The three-dimensional Hénon model. We choose $\xi_0 = \begin{pmatrix} 0.2 & 0.1 & 0 \end{pmatrix}^\top$ as initial point and obtain the spectral intervals

$$\mathcal{I}_1 = [1.3967, 1.4588] \quad \text{and} \quad \mathcal{I}_2 = [0.3113, 0.3919].$$

The corresponding unstable fibers $\mathcal{W}_k^1 = T_{\xi_k}\mathcal{F}_k^u$ are one-dimensional and the stable fibers $\mathcal{W}_k^2 = T_{\xi_k}\mathcal{F}_k^s$ are two-dimensional. These subspaces are shown in Figure 4.3 for $81 \leq k \leq 85$.

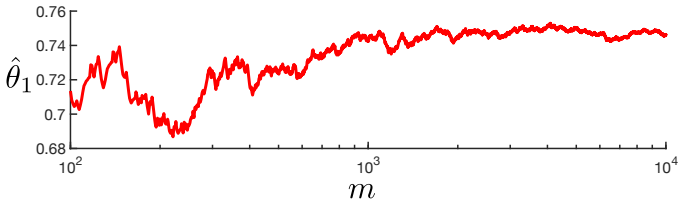

Figure 4.2: Angular value $\hat{\theta}_1$ in the two-dimensional Hénon model, computed for $k = 50$ and $m \in [10^2, 10^4] \cap \mathbb{N}$.

The angular value $\hat{\theta}_1 = 0.8129$ is attained in $\mathcal{W}_k^1$:

$$\theta_1(\mathcal{W}_k^1) = 0.8129, \quad \max_{x \in \mathcal{B}_k^2} \theta_1(x) = 0.7064.$$

While the first angular value $\hat{\theta}_1$ describes the angle between successive unstable tangent spaces $T_{\xi_k}\mathcal{F}_k^u$ on average, the average angle between successive stable tangent spaces $T_{\xi_k}\mathcal{F}_k^s$ is given by the second angular value $\hat{\theta}_2 = 0.8432$, see Figure 4.3. This is justified by our numerical computations

$$\theta_2(\mathcal{W}_k^2) = 0.8432, \quad \max_{x \in \mathcal{B}_k^2} \theta_2(\mathcal{W}_k^1 \oplus \operatorname{span}(x)) = 0.6352.$$

Note that generally, angular values are not attained within stable respectively unstable subspaces. Therefore, the three-dimensional Hénon model seems to be exceptional in this regard. In general, invariant subspaces (in a nonautonomous sense) in which angular values are attained, are not characterized by contracting or expanding dynamics, see Section 4.2.3.

4.2.5. A three-dimensional parameter dependent model. We construct a three-dimensional nonautonomous model, which allows an explicit study of angular values. It particularly illustrates that angular values do not necessarily depend on stability properties of the system.

Consider the parameter dependent model for $\varphi = \frac{1}{3}$ and $p > 0$

$$A_n = T^{1,2}_{\varphi(n+1)} \cdot \begin{pmatrix} \frac{1}{2} & 0 & 0 \\ 0 & p & 0 \\ 0 & 0 & 3 \end{pmatrix} \cdot T^{1,2}_{-\varphi \cdot n} \text{ with } T^{1,2}_{\varphi} = \begin{pmatrix} \cos\varphi & -\sin\varphi & 0 \\ \sin\varphi & \cos\varphi & 0 \\ 0 & 0 & 1 \end{pmatrix}. \tag{4.6}$$

$p = \frac{1}{2}$**.** We numerically obtain the spectral intervals $\mathcal{I}_1 = [3, 3]$ and $\mathcal{I}_2 = [\frac{1}{2}, \frac{1}{2}]$ and the first angular value

$$\theta_1(\mathcal{W}_k^1) = 0, \quad \max_{x \in \mathcal{B}_k^2} \theta_1(x) = \frac{1}{3}, \quad \hat{\theta}_1 = \frac{1}{3},$$

as well as the second angular value

$$\theta_2(\mathcal{W}_k^2) = 0, \quad \max_{x \in \mathcal{B}_k^2} \theta_2(\mathcal{W}_k^1 \oplus \operatorname{span}(x)) = \frac{1}{3}, \quad \hat{\theta}_2 = \frac{1}{3},$$

cf. Figure 4.4. Note that the subspaces, in which the maximum is attained are not unique. The component in $\mathcal{W}_k^2$ can be chosen arbitrarily.

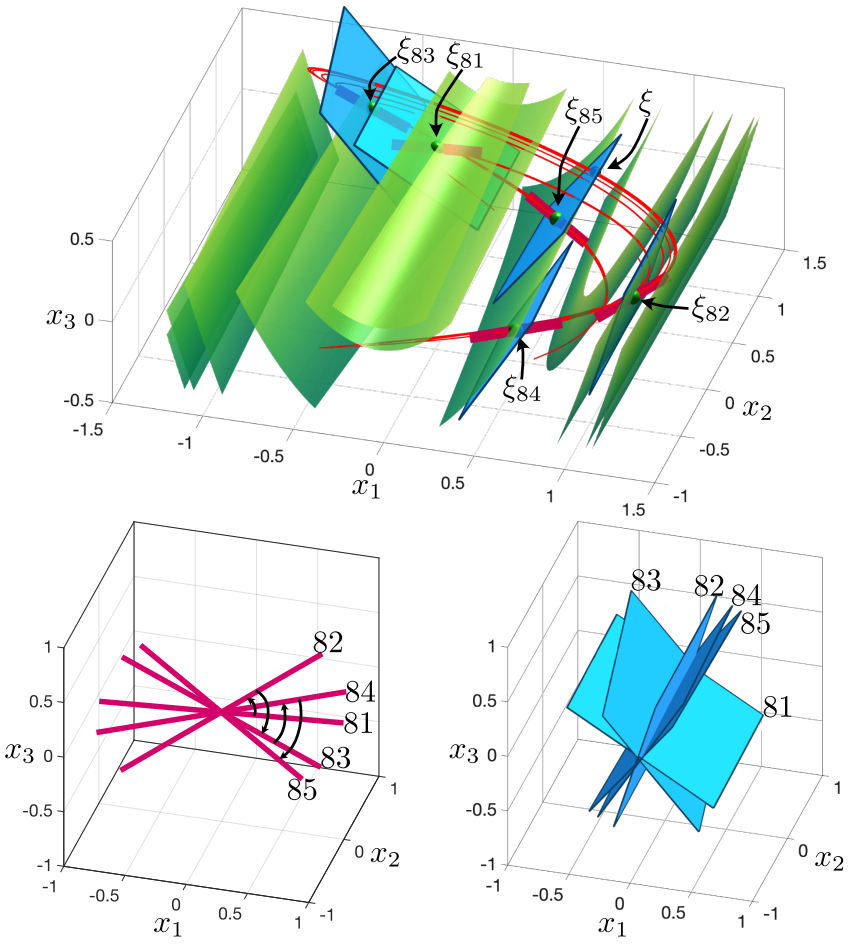

Figure 4.3: Upper panel: Stable (green) and unstable (red) manifolds of the fixed point ξ of the three-dimensional Hénon model. Lower panel: Successive one-dimensional unstable (left) and two-dimensional stable (right) tangent spaces.

$p = 2$. In this example, we obtain three spectral intervals $\mathcal{I}_1 = [3, 3]$, $\mathcal{I}_2 = [1.9955, 2.0000]$ and $\mathcal{I}_3 = [0.5000, 0.5011]$. We observe that

$$\theta_1(\mathcal{W}_k^1) = 0, \quad \theta_1(\mathcal{W}_k^2) = \frac{1}{3}, \quad \theta_1(\mathcal{W}_k^3) = \frac{1}{3}.$$

Thus $\hat{\theta}_1 = \frac{1}{3}$, where the maximum is attained for two fibers. In Figure 4.5, the algorithm chooses $\mathcal{W}_k^3$.

The second angular value is also attained for two trace spaces

$$\theta_2(\mathcal{W}_k^1 \oplus \mathcal{W}_k^2) = \frac{1}{3}, \quad \theta_2(\mathcal{W}_k^1 \oplus \mathcal{W}_k^3) = \frac{1}{3}, \quad \theta_2(\mathcal{W}_k^2 \oplus \mathcal{W}_k^3) = 0, \quad \hat{\theta}_2 = \frac{1}{3}.$$

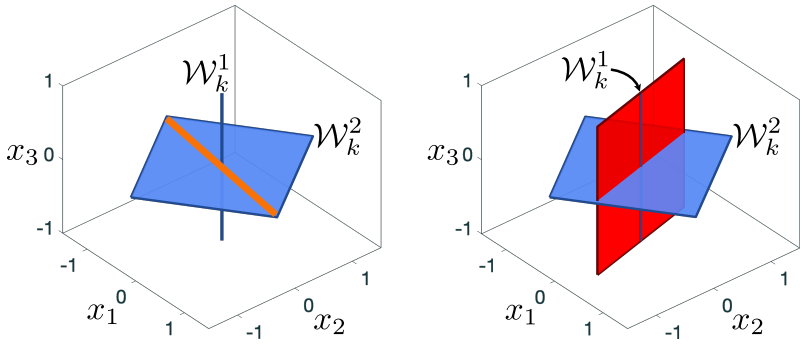

Figure 4.4: Spectral bundles (blue) of (4.6) for $k = 51$ and $p = \frac{1}{2}$. The angular values $\hat{\theta}_{1,2}$ are attained at subspaces which are shown in red.

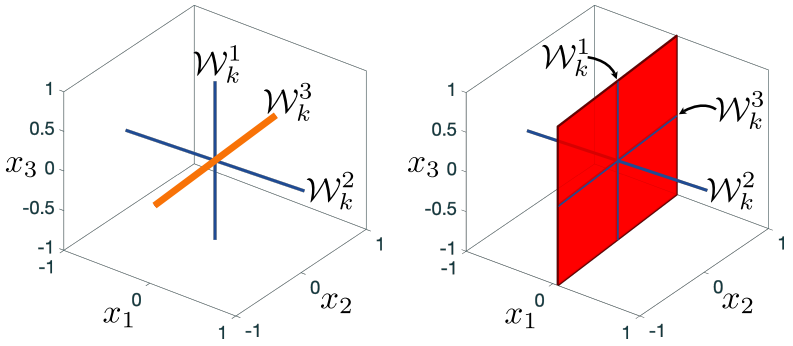

Figure 4.5: Spectral bundles (blue) of (4.6) for $k = 51$ and $p = 2$. The angular values $\hat{\theta}_{1,2}$ are attained at subspaces which are shown in red.

4.2.6. A random dynamical system. For $\varphi = 0.2$, we define

$$B_1 = \begin{pmatrix} 2\cos(\varphi) & -2\sin(\varphi) & 0 \\ 2\sin(\varphi) & 2\cos(\varphi) & 0 \\ 0 & 0 & 3 \end{pmatrix}, \quad B_2 = \begin{pmatrix} 1 & 0 & 0 \\ 0 & 1 & 0 \\ 0 & 0 & 5 \end{pmatrix}$$

and construct the 3-dimensional random dynamical system

$$A_n = B_r, \qquad \text{where } r \in \{1, 2\} \text{ is uniformly distributed for each } n \in \mathbb{N}.$$

This random dynamical system allows an explicit study of the dichotomy spectrum, see [1, Remark 4.2.9], and of angular values. $\Sigma_{\mathrm{ED}} = \{\lambda_1, \lambda_2\}$ with

$$\lambda_1 = \sqrt{3 \cdot 5} \approx 3.872, \quad \lambda_2 = \sqrt{1 \cdot 2} \approx 1.414$$

and corresponding trace spaces are

$$\mathcal{W}_k^1 = \operatorname{span} \begin{pmatrix} 0 \\ 0 \\ 1 \end{pmatrix}, \quad \mathcal{W}_k^2 = \operatorname{span} \left(\begin{pmatrix} 1 \\ 0 \\ 0 \end{pmatrix}, \begin{pmatrix} 0 \\ 1 \\ 0 \end{pmatrix} \right).$$

First and second angular values are equal to 1, since

$$\theta_1(\mathcal{W}_k^1) = 0, \quad \forall x \in \mathcal{B}_k^2 : \theta_1(x) = \frac{0.2 + 0}{2} = 0.1$$

and

$$\theta_2(\mathcal{W}_k^2) = 0, \quad \forall x \in \mathcal{B}_k^2 : \theta_2(\mathcal{W}_k^1 \oplus \operatorname{span}(x)) = 0.1.$$

These analytic results are in coincidence with the output of our numerical algorithm. One realization gives the spectral intervals $\mathcal{I}_1 = [3.86, 3.92]$ and $\mathcal{I}_2 = [1.39, 1.42]$ and the first angular value

$$\theta_1(\mathcal{W}_k^1) = 0, \quad \max_{x \in \mathcal{B}_k^2} \theta_1(x) = 0.099631 = \hat{\theta}_1.$$

A numerical computation of the second angular value yields

$$\theta_2(\mathcal{W}_k^2) = 0, \quad \max_{x \in \mathcal{B}_k^2} \theta_2(\mathcal{W}_k^1 \oplus \operatorname{span}(x)) = 0.099631 = \hat{\theta}_2.$$

4.2.7. Coupled oscillators. We consider a canonical model for two nonlinear oscillators, where these oscillators are linearly coupled with diffusion-like coupling. This ODE-model originates from [3], see also [13, 12]:

$$x' = G(x), \quad G(x) = \begin{pmatrix} x_1 + p_1 x_2 - (x_1^2 + x_2^2)x_1 - \lambda(x_1 + x_2 - x_3 - x_4) \\ -p_1 x_1 + x_2 - (x_1^2 + x_2^2)x_2 - \lambda(x_1 + x_2 - x_3 - x_4) \\ x_3 + p_2 x_4 - (x_3^2 + x_4^2)x_3 + \lambda(x_1 + x_2 - x_3 - x_4) \\ -p_2 x_3 + x_4 - (x_3^2 + x_4^2)x_4 + \lambda(x_1 + x_2 - x_3 - x_4) \end{pmatrix} \tag{4.7}$$

with parameters $p_1 = 0.1$ and $p_2 = 0.55$. Let $F : \mathbb{R}^4 \to \mathbb{R}^4$ be the 1-flow of (4.7). As in Section 4.2.3 we determine angular values for the variational equation along an F-orbit. For computing the 1-flow, we apply the explicit Euler scheme with step size $h = 0.01$. With initial value $\xi_0 = \begin{pmatrix} 1 & 0 & 1 & 0 \end{pmatrix}^\top$, we compute F-orbits of length $M = 1000$ for $\lambda \in \{0, 0.05, 0.2, 0.5\}$, see Figure 4.6. For illustrating our algorithm, angular values

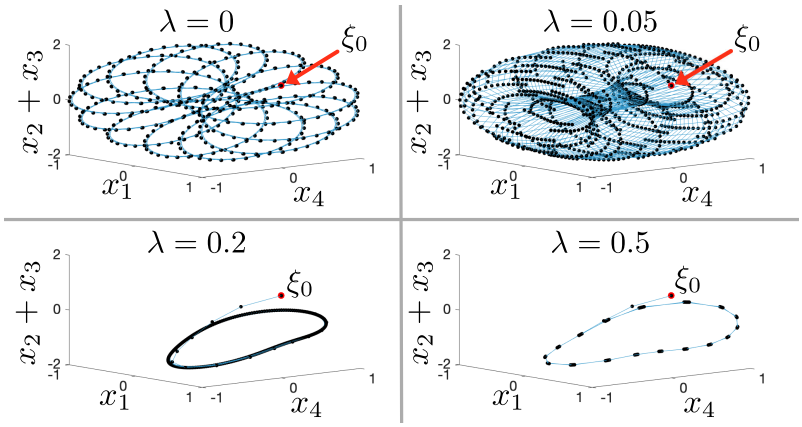

Figure 4.6: Orbit segments of length $M = 1000$ of the 1-flow of (4.7) for various values of the coupling parameter λ.

are presented for all trace spaces. These trace spaces are depicted in Figure 4.7. In

both diagrams, we project the $\mathbb{R}^4$ to the three-dimensional $(x_1, x_4, x_2 + x_3)$ space. This projection preserves the dimension and the linear structure of the subspaces, displayed in Figure 4.7.

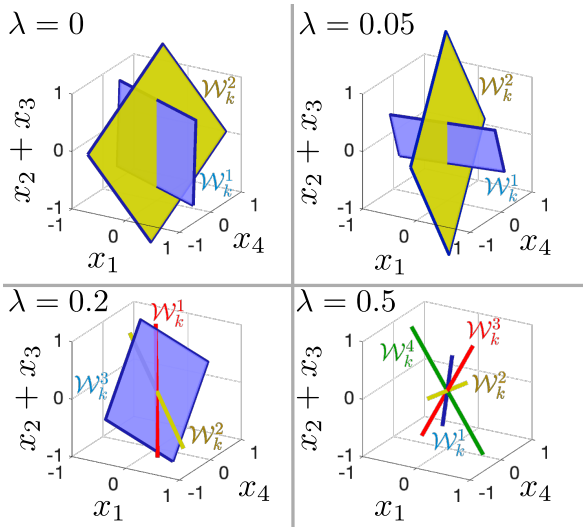

Figure 4.7: Trace spaces of (4.7), computed for $k = 51$ and various values of the coupling parameter λ.

$\lambda = 0$. The spectral intervals are $\mathcal{I}_1 = [0.98, 1.00]$, $\mathcal{I}_2 = [0.132, 0.134]$, $\dim(\mathcal{W}_k^1) = \dim(\mathcal{W}_k^2) = 2$ and the first angular value is

$$\hat{\theta}_1 = \max_{x \in \mathcal{B}_k^1} \theta_1(x) = 0.550003 = \max_{x \in \mathcal{B}_k^2} \theta_1(x).$$

The second angular value is given by

$$\hat{\theta}_2 = \theta_2(\mathcal{W}_k^1) = 0.550003 = \theta_2(\mathcal{W}_k^2) = \max_{x \in \mathcal{B}_k^1,\ y \in \mathcal{B}_k^2} \theta_2(\operatorname{span}(x, y)).$$

Note that for $\lambda = 0$, we have the block matrix $DG(x) = \begin{pmatrix} H_{1,2}(x) & 0 \\ 0 & H_{3,4}(x) \end{pmatrix}$ with

$$H_{i,j}(x) = \begin{pmatrix} 1 - 3x_i^2 - x_j^2 & p_{\min(i,2)} - 2x_i x_j \\ -p_{\min(i,2)} - 2x_i x_j & 1 - x_i^2 - 3x_j^2 \end{pmatrix} \text{ for } (i,j) \in \{(1,2), (3,4)\}.$$

But the intuitive conjecture that each $H_{i,j}$ generates one spectral interval turns out to be wrong. Indeed, we get for $k = 51$

$$\mathcal{W}_k^1 = \operatorname{span}\left(\begin{pmatrix} 0.352 \\ -0.144 \\ -0.206 \\ 0.902 \end{pmatrix}, \begin{pmatrix} 0.856 \\ -0.350 \\ 0.085 \\ -0.370 \end{pmatrix} \right), \quad \mathcal{W}_k^2 = \operatorname{span}\left(\begin{pmatrix} 0.374 \\ 0.918 \\ 0.128 \\ 0.030 \end{pmatrix}, \begin{pmatrix} -0.049 \\ -0.121 \\ 0.965 \\ 0.226 \end{pmatrix} \right).$$

$\lambda = 0.05$. We obtain the spectral intervals $\mathcal{I}_1 = [0.993, 1.001]$, $\mathcal{I}_2 = [0.146, 0.147]$, $\dim(\mathcal{W}_k^1) = \dim(\mathcal{W}_k^2) = 2$,

$$\hat{\theta}_1 = \max_{x \in \mathcal{B}_k^1} \theta_1(x) = 0.5389, \ \max_{x \in \mathcal{B}_k^2} \theta_1(x) = 0.5157$$

and

$$\hat{\theta}_2 = \theta_2(\mathcal{W}_k^1) = 0.53901 = \theta_2(\mathcal{W}_k^2), \quad \max_{x \in \mathcal{B}_k^1,\ y \in \mathcal{B}_k^2} \theta_2(\mathrm{span}(x, y)) = 0.5262.$$

$\lambda = 0.2$. In this case, we get 3 spectral intervals $\mathcal{I}_1 = [0.99, 1.00]$, $\mathcal{I}_2 = [0.703, 0.705]$, $\mathcal{I}_3 = [0.13, 0.16]$, $\dim(\mathcal{W}_k^1) = \dim(\mathcal{W}_k^2) = 1$, $\dim(\mathcal{W}_k^3) = 2$ with angular values

$$\hat{\theta}_1 = \theta_1(\mathcal{W}_k^1) = 0.452, \ \theta_1(\mathcal{W}_k^2) = 0.409, \ \max_{x \in \mathcal{B}_k^3} \theta_1(\mathrm{span}(x)) = 0.401$$

and

$$\begin{aligned} \hat{\theta}_2 &= \theta_2(\mathcal{W}_k^1 \oplus \mathcal{W}_k^2) = 0.443, \\ &\max_{x \in \mathcal{B}_k^3} \theta_2(\mathcal{W}_k^1 \oplus \mathrm{span}(x)) = 0.301, \ \max_{x \in \mathcal{B}_k^3} \theta_2(\mathcal{W}_k^2 \oplus \mathrm{span}(x)) = 0.403. \end{aligned}$$

$\lambda = 0.5$. For this coupling, we find 4 spectral intervals $\mathcal{I}_1 = [0.99, 1.00]$, $\mathcal{I}_2 = [0.342, 0.347]$, $\mathcal{I}_3 = [0.1683, 0.1698]$, $\mathcal{I}_4 = [0.0609, 0.0615]$, $\dim(\mathcal{W}_k^1) = \dim(\mathcal{W}_k^2) = \dim(\mathcal{W}_k^3) = \dim(\mathcal{W}_k^4) = 1$ with angular values

$$\hat{\theta}_1 = \theta_1(\mathcal{W}_k^2) = 0.44, \ \theta_1(\mathcal{W}_k^1) = 0.41, \ \theta_1(\mathcal{W}_k^3) = 0.43, \ \theta_1(\mathcal{W}_k^4) = 0.39$$

and

$$\begin{aligned} \hat{\theta}_2 = \theta_2(\mathcal{W}_k^1 \oplus \mathcal{W}_k^4) = 0.515, \ \theta_2(\mathcal{W}_k^1 \oplus \mathcal{W}_k^2) = 0.453, \\ \theta_2(\mathcal{W}_k^1 \oplus \mathcal{W}_k^3) = 0.333, \ \theta_2(\mathcal{W}_k^2 \oplus \mathcal{W}_k^3) = 0.468, \\ \theta_2(\mathcal{W}_k^2 \oplus \mathcal{W}_k^4) = 0.501, \ \theta_2(\mathcal{W}_k^3 \oplus \mathcal{W}_k^4) = 0.463. \end{aligned}$$

Finally we note that this model particularly illustrates that all cases $\hat{\theta}_1 \left\{ \begin{matrix} < \\ = \\ > \end{matrix} \right\} \hat{\theta}_2$ may occur.

Acknowledgments. Both authors are grateful to the Research Centre for Mathematical Modelling (RCM^2) at Bielefeld University for continuous support of their joint research. For further support, WJB thanks the CRC 1283 "Taming uncertainty and profiting from randomness and low regularity in analysis, stochastics and their applications" and TH thanks the Faculty of Mathematics at Bielefeld University.

REFERENCES

[1] L. Arnold. *Random dynamical systems.* Springer Monographs in Mathematics. Springer-Verlag, Berlin, 1998.

[2] L. Arnold and L. San Martin. A multiplicative ergodic theorem for rotation numbers. *J. Dynam. Differential Equations*, 1(1):95–119, 1989.

[3] D. G. Aronson, E. J. Doedel, and H. G. Othmer. An analytical and numerical study of the bifurcations in a system of linearly-coupled oscillators. *Phys. D*, 25(1-3):20–104, 1987.

[4] B. Aulbach and J. Kalkbrenner. Exponential forward splitting for noninvertible difference equations. *Comput. Math. Appl.*, 42(3-5):743–754, 2001.

[5] B. Aulbach and S. Siegmund. The dichotomy spectrum for noninvertible systems of linear difference equations. *J. Differ. Equations Appl.*, 7:895–913, 2001.

[6] W.-J. Beyn, G. Froyland, and T. Hüls. Angular values of nonautonomous and random linear dynamical systems. Technical report, Department of Mathematics, Bielefeld University, 2020.

[7] W.-J. Beyn and J.-M. Kleinkauf. Numerical approximation of homoclinic chaos. *Numer. Algorithms*, 14:25–53, 1997.

[8] W. A. Coppel. *Dichotomies in Stability Theory*. Springer, Berlin, 1978. Lecture Notes in Mathematics, Vol. 629.

[9] J. L. Daleckiĭ and M. G. Kreĭn. *Stability of Solutions of Differential Equations in Banach Space*. American Mathematical Society, Providence, R.I., 1974.

[10] W. de Melo and S. van Strien. *One-dimensional dynamics*, volume 25 of *Ergebnisse der Mathematik und ihrer Grenzgebiete (3)*. Springer-Verlag, Berlin, 1993.

[11] L. Dieci, C. Elia, and E. Van Vleck. Exponential dichotomy on the real line: SVD and QR methods. *J. Differential Equations*, 248(2):287–308, 2010.

[12] L. Dieci and J. Lorenz. Computation of invariant tori by the method of characteristics. *SIAM J. Numer. Anal.*, 32(5):1436–1474, 1995.

[13] L. Dieci, J. Lorenz, and R. D. Russell. Numerical calculation of invariant tori. *SIAM J. Sci. Statist. Comput.*, 12(3):607–647, 1991.

[14] D. E. Edmunds and W. D. Evans. *Spectral theory and differential operators*. Oxford mathematical monographs. Clarendon Press, Oxford, repr. (with corr.), digital print. edition, 2002.

[15] G. H. Golub and C. F. Van Loan. *Matrix computations*. Johns Hopkins Studies in the Mathematical Sciences. Johns Hopkins University Press, Baltimore, MD, fourth edition, 2013.

[16] M. Hénon. A two-dimensional mapping with a strange attractor. *Comm. Math. Phys.*, 50(1):69–77, 1976.

[17] D. Henry. *Geometric Theory of Semilinear Parabolic Equations*. Springer, Berlin, 1981.

[18] T. Hüls. Computing Sacker-Sell spectra in discrete time dynamical systems. *SIAM J. Numer. Anal.*, 48(6):2043–2064, 2010.

[19] T. Hüls. Computing stable hierarchies of fiber bundles. *Discrete Contin. Dyn. Syst. Ser. B*, 22(9):3341–3367, 2017.

[20] T. Hüls and C. Pötzsche. Qualitative analysis of a nonautonomous Beverton-Holt Ricker model. *SIAM J. Appl. Dyn. Syst.*, 13(4):1442–1488, 2014.

[21] S. Jiang. Angles between Euclidean subspaces. *Geom. Dedicata*, 63(2):113–121, 1996.

[22] J. Kalkbrenner. *Exponentielle Dichotomie und chaotische Dynamik nichtinvertierbarer Differenzengleichungen*, volume 1 of *Augsburger Mathematisch-Naturwissenschaftliche Schriften*. Dr. Bernd Wißner, Augsburg, 1994.

[23] A. B. Katok and B. Hasselblatt. *Introduction to the modern theory of dynamical systems*. Encyclopedia of mathematics and its applications ; vol. 54. Cambridge University Press, Cambridge, 1995.

[24] Z. Nitecki. *Differentiable dynamics. An introduction to the orbit structure of diffeomorphisms*. The M.I.T. Press, Cambridge, Mass.-London, 1971.

[25] O. Perron. Die Stabilitätsfrage bei Differentialgleichungen. *Math. Z.*, 32(1):703–728, 1930.

[26] C. Pötzsche. Dichotomy spectra of triangular equations. *Discrete Contin. Dyn. Syst.*, 36(1):423–450, 2016.

[27] R. J. Sacker and G. R. Sell. A spectral theory for linear differential systems. *J. Differential Equations*, 27(3):320–358, 1978.

[28] R. E. Vinograd. On a criterion of instability in the sense of Lyapunov of the solutions of a linear system of ordinary differential equations. *Doklady Akad. Nauk SSSR (N.S.)*, 84:201–204, 1952.